# LUND UNIVERSITY

**Interactions and coherences in electron transport through serially coupled quantum dots**

Goldozian, Bahareh

2019

*Document Version:*
Publisher's PDF, also known as Version of record

[Link to publication](Link to publication)

*Total number of authors:*
1

# Interactions and Coherences in Electron Transport Through Serially Coupled Quantum Dots

**BAHAREH GOLDOZIAN | FACULTY OF SCIENCE | LUND UNIVERSITY**
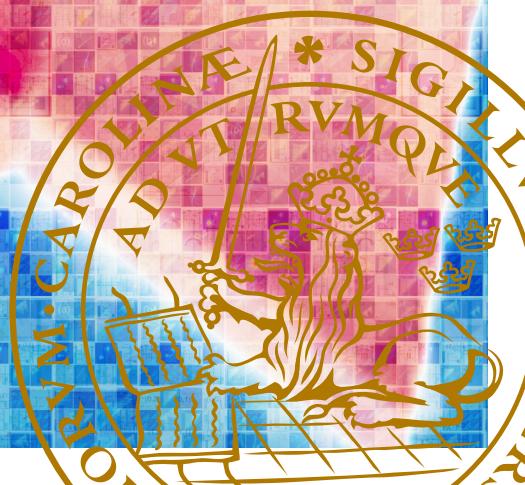
Interactions and Coherences in Electron Transport Through Serially Coupled Quantum Dots

# Interactions and Coherences in Electron Transport Through Serially Coupled Quantum Dots

by Bahareh Goldozian

## LUND
### UNIVERSITY

Thesis for the degree of Doctor of Philosophy in Engineering
Thesis advisors: Assoc. Prof. Peter Samuelsson, Assoc. Prof. Adam Burke
Faculty opponent: Prof. Jonas Fransson

Author(s)
Bahareh Goldozian

Title and subtitle
Interactions and Coherences in Electron Transport Through Serially Coupled Quantum Dots

Abstract

This thesis is considering various aspects of electronic transport through quantum dots, with the focus on two or three dots coupled in series.

In paper I, we study the impact of electron-electron interactions on transport in a system of triple quantum dots with spin. We show that due to electron-electron scattering processes, transport is possible beyond the common single-particle transmission channels. We also check the validity of the Pauli master equation by comparing it with the first-order von Neumann approach.

In paper II, we report the addition of phonon scattering to the recently established numerical package QmeQ for transport in quantum dot systems. Also, we analyze phonon-assisted transport in the absence of applied source-drain voltage.

In paper III, we present a combined experimental and theoretical study of a nanowire double quantum dot system. We investigate the origin and properties of the bias triangle features and predict and observe features directly related to the inter-dot exchange energy.

In paper IV, based on what was presented in paper II, it is shown that by coupling a hot phonon bath to a double quantum dot, phonon assisted transport can be used to drive currents through the double dot and effectively harvest energy from the phonon bath.

Key words
Quantum transport, Pauli spin blockade, double quantum dot, phonon assisted transport, thermoelectrics

Classification system and/or index terms (if any)

Signature _Goldozian_ (signature)

Date    2019-03-13

DOKUMENTDATABLAD enl SIS 61 41 21

# Interactions and Coherences in Electron Transport Through Serially Coupled Quantum Dots

by Bahareh Goldozian

LUND
UNIVERSITY

A doctoral thesis at a university in Sweden takes either the form of a single, cohesive research study (monograph) or a summary of research papers (compilation thesis), which the doctoral student has written alone or together with one or several other author(s).

In the latter case the thesis consists of two parts. An introductory text puts the research work into context and summarizes the main points of the papers. Then, the research publications themselves are reproduced, together with a description of the individual contributions of the authors. The research papers may either have been already published or are manuscripts at various stages (in press, submitted, or in draft).

**Cover illustration front:** Phonon assistant current in a double quantum dot system.

# Contents

# List of publications and contributions of the author

This thesis is based on the following publications, referred to by their Roman numerals:

   I   **Transport in serial spinful multiple-dot systems: The role of electron-electron interactions and coherences**

B.Goldozian, F.A. Damtie, G. Kiršanskas, and A. Wacker
Sci. Rep. **6**, 22761 (2016)

We study the impact of electron-electron interactions on transport in a spinful serial triple quantum dot system weakly coupled to two leads. We find that due to electron-electron scattering processes, the transport is enabled beyond the common single-particle transmission channels. Additionally, we check the validity of the Pauli master equation by comparing it with the first-order von Neumann approach and demonstrate that coherences are of relevance if the energy spacing of the eigenstates is smaller than the lead transition rate multiplied by $\hbar$.

*Contribution*: I did all the calculations and drew all the figures. I also wrote the first draft of the manuscript in collaboration with the co-authors and contributed to its final writing.

   II   **Quantifying the impact of phonon scattering on electrical and thermal transport in quantum dots**

B.Goldozian, G. Kiršanskas, F.A. Damtie, and A. Wacker
Eur. Phys. J. Spec. Top. **227**, 1959 (2019)

We report the inclusion of phonon scattering to our recently established numerical package QmeQ for transport in quantum dot systems. This enables straightforward calculations for a large variety of devices. As examples we show (i) transport in a double-dot structure, where energy relaxation is crucial to match the energy difference between the levels, and (ii) the generation of electrical power by contacting cold electric contacts with quantum dot states, which are subjected to heated phonons.

*Contribution*: I did most of the calculations and drew all the figures. I also wrote the first draft of the manuscript in collaboration with the co-authors and contributed to its final writing.

III **Bias triangle features in enhancement mode InAs nanowire double quantum dots**

B.Goldozian, S. Dorsch, S. Fahlvik, P. Samuelsson, A. Wacker, A. Burke

(Manuscript in preparation)

Here we show, by combining electrical current measurements, quantitative transport numerics, and a qualitative model, that new features that are observed in the bias triangles are a manifestation of intra-dot exchange interaction. We also provide conditions for the observations of the features in terms of dot-reservoir coupling asymmetry, inter-dot coupling strength, and electron-phonon interactions. Our findings provide a novel way to determine the exchange interaction directly from the bias triangles.

*Contribution*: I did most of the calculations and obtained the data for all the plots. I prepared the first draft of the manuscript and contributed to the discussions of the results.

IV **Heat driven transport in serial double quantum dot devices**

S. Dorsch, A. Svilans, M. Josefsson B.Goldozian, M. Kumar, C. Thelander, A. Wacker, and A. Burke

(Manuscript in preparation)

We present controlled studies of thermal interactions with epitaxially-defined DQDs to gain vital insights into parasitic, temperature induced currents in different interdot tunnel coupling regimes. Metal plunger gates and a side-heater are placed in close vicinity to the contacted nanowire. The finite bias spectroscopy with measurements at no source-drain bias were combined, to study the effect of thermal gradients and phonon assisted transport in DQD devices.

*Contribution*: Based on the calculation I did for the second paper, the idea of this work was developed. I performed some of the calculations and participated in the discussions of the formulation of the manuscript.

All papers are reproduced with permission of their respective publishers.

# Acknowledgements

# Popular summary in English

Quantum mechanics has become the most successful framework in the history of science, and our modern life is based on it. Quantum mechanics provides the physics behind almost every technology that makes the modern world what it is today: computers, communication technology, cellphones, and the internet are all based on that. After the invention of the light bulb by Thomas Alva Edison in 1879, scientists got interested in the properties of the light that is given off by materials as they are heated. So they started to study the tiniest building blocks of nature like atoms or molecules. They designed several clever experiments, and they played with light interacting with matter. They found that what they observed in those experiments, can not be explained with the physics that they were familiar with. Hence they invented new physical laws of nature. These new laws are based on the principles of quantum mechanics, which are different from how we experience the world in our daily lives.

In the last decades, there has been an accelerated demand and huge research interest to find better alternatives to traditional and typical devices. Therefore researchers were encouraged to develop the experimental technique as well as the theoretical tools toward smaller and smaller components. For instance, they try to build faster and more powerful computers; therefore, they make smaller transistors to be able to pack many of them into a small space so they can "talk to each other." Today we have nanometer-scale devices, which are only around 100 times larger than atoms. These nanodevices show new behaviors, and what makes them exciting is the fact that we need quantum mechanics to describe these behaviors.

Thus it is essential to improve our theoretical tools to investigate different properties of the nanostructures and gain a better understanding of these effects. My project is studying the electron transport in the nanostructures theoretically. Improving the theoretical tools and investigating the thermal and electrical properties of the nanostructures will allow us to make more efficient devices.

For example, nanotechnology has great potential for applications in the field of renewable energy. One of the most eco-friendly energy sources, which is usually attainable, almost everywhere, is the thermal energy. Also, It is known that thermal energy can be converted into electrical current. Thus one can use heat and get electrical current, which is the physical concept behind the ongoing energy technologies, such as heat engines. The thermal and electrical properties of the nanowires allow us to make the energy conversion process more and more efficient. Since a lot of heat is lost to the environment, this concept will be fundamental, beneficial, and helpful in our modern industrial world. Taking advantage of heat to create electricity will decrease the mass of carbon emissions and also reduce pollution.

Some companies have been working on producing a "smart watch". A dream product: a watch with a battery that never needs to be charged by extend devices. The body heat and solar energy do this job so long as the watch is being worn. In reference [1] the authors describe the design of a watch that is equipped with a thermoelectric engine, that harvest human body heat, converts it to electricity and generates the required voltage to charge the battery of the watch.

# Part I

# Introduction, background and theory

# Chapter 1

# Introduction

The impressive development of high precision fabrication in the last few decades has made it possible to design semiconductor structures in a very small size to such an extent that the electrons are confined in one, two, or three dimensions. These fabricated objects, with structures at the nanoscale, are known as nanostructures. For such small devices, however, the charge transport is dominated by quantum effects such as discrete energy levels, electron tunneling, and non-classical interferences. While these effects make a further downsizing of semiconductors difficult, they offer the possibility of nanoelectronic devices based on them. Such devices, which could consist of a single atom or molecule, would allow for a leap in chip manufacturing at the nanoscale. Possible applications are on the one hand to build integrated circuits for classical computers, which would pave the way for a much faster and more energy-efficient computing. On the other hand, nanoelectronic devices might also provide a basis for future on-chip quantum computing. Depending on the dimensions in which the electrons are confined, one can classify nanostructures as quantum layers [2], quantum wires [3, 4] or nanowires [5, 6], and quantum dots.

A promising approach to build fully functional nanoelectronic devices is to utilize the so-called quantum dot. Quantum dots (QDs) are capable of confining the electrons in all three spatial dimensions. QDs behave as artificial atoms where the confinement potential substitutes the nuclear potential [7, 8]. A striking feature of quantum dots is that they act like single atoms in many respects [9]. Nonetheless, in contradistinction to atoms, quantum dots are highly tunable [10] and it is possible to grow them in a way to be able to control various characteristics of them such as the confinement potential, electron density as well as to adjust the energy level positions electrostatically [11, 12]. Recent developments in fabricating nanoelectronic devices have heightened the need for better techniques to simulate quantum transport through these devices.

This thesis is devoted to a better theoretical understanding of transport in nanostructures, where the nanostructures treated are quantum dots systems. A better knowledge of the transport through such systems is expected to facilitate the development of more functional electronic devices. The work presented in this thesis is a theoretical study, focusing mainly on the effect of interactions in nanosystems. We investigate the influence of electron-electron interactions on transport in a system of serial triple quantum dots. We find that due to electron-electron scattering processes, the transport is enabled beyond the common single-particle transmission channels. We also check the validity of the Pauli master equation by comparing it with the first-order von Neumann approach (Paper I).

Moreover, we report the addition of phonon scattering to recently established numerical package QmeQ for transport in quantum dot systems. Also, we propose and investigate phonon assisted transport in the absence of the source-drain voltage (Paper II). We present a combined experimental and theoretical study of the nanowire double quantum dot. We investigate the origin and properties of the bias triangle features and predict and observe features directly related to the inter-dot exchange energy (Paper III). Also, from results presented in paper II together with experimental colleagues, it was shown that by coupling a hot phonon bath to the double quantum dot, phonon assisted transport could be used to drive currents through a double quantum dot in a three-terminal geometry, and effectively harvest energy from the phonon bath (Paper IV).

The thesis is organized as follows. In chapter 2, I will give a general explanation of the physical properties and features of single and double-dot systems, and describe the triple-dot system which we have studied in paper III. In chapter 3, a general model system, the Hamiltonian and different interactions will be discussed. In chapter 4 we will take a brief look at the numerical method used in the calculations. In chapter 5 the main results of the papers will be summarized. A summary and outlook are given in chapter 6. Finally, the papers are reprinted at the end of the thesis.

# Chapter 2

# Quantum dots

This thesis is considering various aspects of electronic transport through quantum dots, with the focus on two or three dots coupled in series. Quantum dots (QDs) are small, typically of nanometer size, with electronic properties largely determined by the laws of quantum mechanics. QDs have been investigated intensively since the mid-1980s [13, 14] and are still attracting considerable research interest, largely due to the large number of possible applications based on QDs. To mention a few, QDs can be used in light emitting diodes[15] and lasing [16, 17], as quantum technology components in quantum bits [18, 19] and single photon sources [20, 21], and as nanoscale electronic components, for example in single electron transistors [22]. However, due to their inherent quantum mechanical nature, QDs are also widely used as components in basic physics investigations [23].

Typically QDs are made of semiconductor materials, but there are also other types of material used, for example graphene [24]. A wide variety of QD implementations have been demonstrated, in for example lateral [25] and vertical [26] two dimensional electron gas systems, in nanowires [27, 28] and nanotubes [29], and in self-assembled nanodot geometries [30, 31]. The focus in this thesis, in particular in papers III and IV where experimental results are presented, is on semiconductor nanowire QDs made of III-IV material combinations such as InAs, GaP, etc. However, all the theoretical methods and results presented are valid for any type of quantum dots, since they typically depend on generic properties such as tunnel rates, electronic interactions, and energy level structure.

The reason for focusing on nanowire QDs, besides the fact that Lund University has been a world leading institution in nanowire research during the last one and a half decade [6], is that nanowire QDs have many appealing properties. In particular, the material composition [32] and even crystal structure [33] can be controlled on atomic distances giving rise to very well defined QDs. Moreover, as is true for many types of QDs, the nanowire

QDs can be coupled to electrical contacts, allowing electrical transport measurements and characterization. Also, by adding electrostatic, metallic gates close to or on top of/under the wires, the electronic properties such as tunnel barrier strengths, electron density, and energy levels can be controlled in-situ, during an experiment.

To provide a compelling illustration of a nanowire QD and the electrical contacting and electrostatic gating, we show in Fig. 2.1(a) the micrograph of the InAs wire device investigate in paper III. From the scanning electron image one clearly sees the InAs nanowire, with
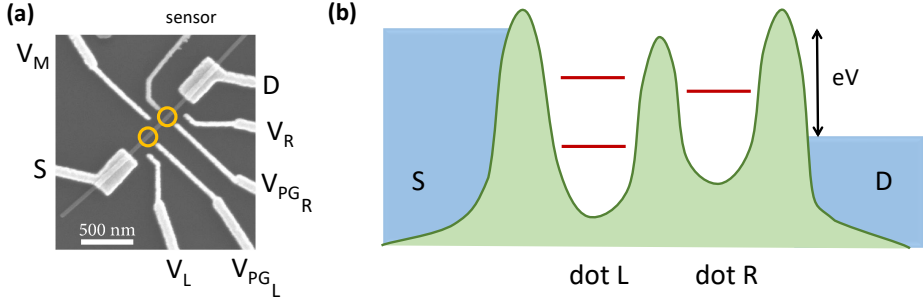


Figure 2.1: (a) Scanning electron image of a nanowire double QD coupled to source (S) and drain (D) contacts, with a number of electrostatic gates (see text for details). The position of the two QDs are shown schematically with yellow circles. The picture is taken from paper III. (b) Schematic electrostatic potential constituting the double QDs, with two (one) single particle levels in the left (right) dot and the chemical potentials of the source and drain contacts, differing by the amount $eV$, where $V$ is the applied source-drain voltage.

a diameters of approximately 35 nm and a length of $5\mu$m. The wire, with a Wurtzite crystal structure, is placed on an Si substrate covered by an electrically insulating layer $SiO_2$. The wire is coupled to two metallic contacts, one acting as source (S) and one as drain (D) for the electrical current flowing through the wire. In addition, there are a set of electrostatic finger gates placed close to the wire, having different functions. The three gates L,M,R, with corresponding applied potentials $V_L$, $V_M$, $V_R$ are used to modify the electrical potential locally in the wire. Applying negative potentials $V_L$, $V_M$, $V_R$ leads to the formation of potential barriers for the electrons. The resulting potential three-barrier structure, shown schematically in Fig. 2.1(b), thus contains two potential wells, effectively constituting two serially coupled quantum dots, one to the left (L) and one to the right (R).

Due to the quantum confinement along the wire, a structure with discrete energy levels are formed in each dot, denoted by thick lines in Fig. 2.1(b). The levels are slightly broadened due to the couplings to the source and drain contacts. The two plunger gates $PG_L$ and $PG_R$ are used to shift the QD levels up/down in energy, by applying negative/positive voltages $V_{PG_L}$ and $V_{PG_R}$ respectively. Finally, there is in Fig. 2.1(b) a gate denoted sensor. It can in principle be used to sense the presence or absence of single electrons in the dots, however, for the discussions in this thesis this type of charge sensing is not used.

A voltage bias $V$ is applied between the source and the drain, allowing electrons to tun-

nel between the dots, giving rise to an electric current. One can also, as is discussed in paper IV, apply different temperatures to the source and drain contacts, in order to investigate thermoelectric phenomena. We stress that, as is the case in essentially all electronic nanostructures, tuning one electrical potential also leads to modifications of all the other potentials due to capacitive cross-talk. In practice it is a non-trivial experimental task to compensate for this effect by tuning all potentials to obtain the desired effect on a single wire potential. This cross-talk, with the corresponding lever arms, is further discussed below. We also note that in the Fig. 2.1(b), only the conduction band, where the electrons transport takes place, is shown.

## 2.1   Single quantum dot - Coulomb blockade

In addition to the properties of a QD discussed above, there is one additional features of fundamental importance: Electrons on a QD repel each other due to the Coulomb interaction, hence, adding an electron to the quantum dot requires *additional energy* to compensate the electrostatic repulsion caused by all the other electrons. When there is insufficient energy of the tunneling electrons to overcome this repulsion the current can not flow. This phenomenon is referred to as Coulomb blockade.

Taking into account both the discrete energy structure of the quantum dots band the Coulomb blockade effects, one is able to describe a large fraction of transport experiments with QDs. As pointed out above, QDs are useful in making electronic devices and, due to their unique electronic properties, have applications in several areas of science. To characterize the electron transport into a quantum dot, one can connect it to two metallic leads, source (S) and drain (D) [34]. The difference between the source and the drain voltages is equal to the applied bias voltage, $V = V_S - V_D$, and the resulting energy window between the chemical potentials of S and D presents the bias window.

To describe qualitative the charge transport through a QD, we consider the scenario in Fig. 2.2. Electrons can tunnel in and out of a dot when the many-body energy level of the dot is situated in the bias window. The energy levels in the dot can be modified by varying the gate voltage. Figure 2.2(a) schematically demonstrates the energy diagram of a quantum dot occupied by $N$ electrons. $\mu_N$ is the chemical potential of the QD containing $N$ electrons, that is the change in the total energy when adding the $N$th electron to the dot,

$$\mu_N = E(N) - E(N-1). \tag{2.1}$$

Here the energy $E(N)$ consists of both the Coulomb energy and the energy level in the dot to which the electron is tunneling. The current can pass through the dot due to the voltage difference between the leads [35]. When the chemical potentials of the leads are below $\mu(N+1)$, the electrons on the leads do not have enough energy to add the $(N+1)$th
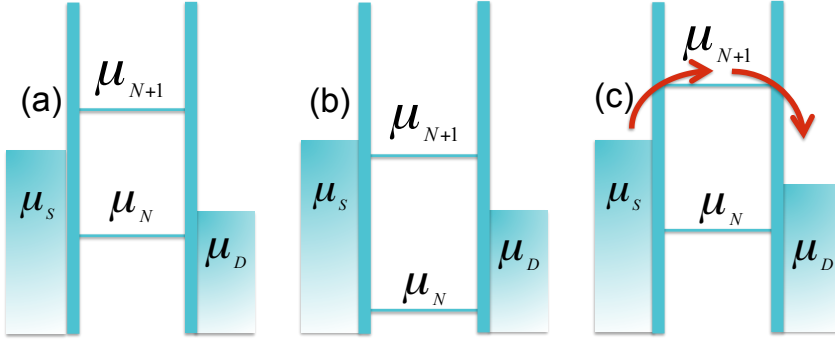
**Figure 2.2:** Schematic model for transport through a single quantum dot. (a) The dot is occupied by $N$ electrons. The $(N+1)th$ electron can neither enter or leave the dot since the chemical potential of the dot is above the chemical potentials the leads (b). By tuning the dot's chemical potential, until the $\mu(N+1)$ is aligned with the chemical potential of the source, the Coulomb blockade is lifted. (c) Schematic energy diagram shows the co-tunneling. The electron uses the dot state as a virtual state, and transport through the dot becomes possible.

electron to the dot. In the same way, when $\mu(N)$ is below the chemical potentials of the leads, the electrons on the dot are not allowed to exit from the dot; therefore the current will be blocked. This phenomenon is known as Coulomb Blockade [36, 37]. The change in the chemical potential required to add an electron to the quantum dot is called the addition energy.

Figure 2.2(b) shows that by changing the dot's chemical potential the Coulomb blockade is lifted and an electron can tunnel into the quantum dot and increase the number of electrons to $N+1$. Meanwhile, this electron is allowed to exit the quantum dot and tunnel through the drain. This transport process, as described here, is known as sequential tunneling. The sequential tunneling is only possible if the energy level of the dot is in the bias window.

Furthermore, electron transport is also possible under some other specific circumstances. Due to the tunneling, the energy level of the dots broadens and gives the electrons of the leads the possibility to transport through energetically forbidden states, outside the bias window, which are known as virtual states. This kind of tunneling is known as co-tunneling process (Fig. 2.2(c)). As a result of the uncertainty relation, electrons can only transport through virtual states if the process happens in short enough time. For this process, the time that the electrons tunnel through the system should be of the same order as the timescale defined by the Heisenberg uncertainty relation. Thus co-tunneling process only happens if there is a strong tunnel coupling between leads and the dot.

Identifying the energy level structure of the quantum dot is essential in order to understand and predict a device performance. A large number of experiments have been done on quantum dots, where with bias spectroscopy [38] or thermoelectric measurements [39], one can obtain the energy level structure.

## 2.2   Single quantum dot - current spectroscopy

Quantum transport through a single dot can be drastically influenced by the quantization of charge and energy. One can obtain spectroscopic information about the charge and the energy levels by analyzing the so-called level spectroscopy diagrams or stability diagrams. The stability plot that exhibits a diamond structure, can be made by measuring the current through the dot, while changing the chemical potential on the leads for different values of the gate voltage. From such plots, one can characterize the electron transport in detail as well as extract parameters such as the distance between the single-particle energy levels and the magnitude of Coulomb interactions.

Figure 2.3 presents an example of such a diagram. The current is plotted as a function of bias, x-axis, $V_b$, and the gate voltage, $V_g$, the y-axis. The bias is changed symmetrically. The Pauli master equation approach is used to calculate the current, as will be explained in Chapter 4. The schematic diagrams (a - d), on the right side of the Fig. 2.3, show the configuration of the electrochemical potentials at different points. As it is illustrated in Fig. 2.3 in the diamond areas along the $V_b$ axis, so-called Coulomb diamonds, no current can flow through the dot, due to the Coulomb blockade effect, and the electron occupation on the dot is fixed. Therefore each diamond corresponds to a determined number of electrons ($N$).

In Fig. 2.3 at point (a), the first chemical potential of the dot is aligned with the source and the drain. The borderline that connects point (a) and (b), shows the alignment of $\mu(1)$ with $\mu_D$. Also, the line that connects (a) and (d) shows the alignment of $\mu(1)$ with $\mu_S$. These lines correspond to the transport onset through the first energy level in the quantum dot. Furthermore, the two lines that connect (b)/(d) and (c) correspond to the alignment of $\mu(2)$ with $\mu_S/\mu_D$.

In general, the points along the edges of each diamond at $V_b = 0$ are the degeneracy points where the chemical potential of the dot, the source, and the drain are aligned. At the diamond borderlines, one of the chemical potentials of the dot is aligned with, either the source or the drain. The second degeneracy point, is the point C, where $\mu(2)$ is aligned with the source and the drain. In the same way, as it was mentioned for point (a), the two bottom borderlines show the transport of the second electron. Nonetheless, this electron is in the same single-particle energy level as in (a) but with opposite spin.

The addition energy can be directly read from the width of the diamond in the source-drain voltage plot, see for example point 'd' in Fig. 2.3. In the experimental data in order to convert the gate voltage to an energy scale one has to know the gate-lever arm, $\alpha_G$. From the ratio of the height and width of a diamond, it is possible to determine the gate lever arms $\alpha_G$. The lateral and vertical sizes of the diamond in Fig. 2.3 are of the same since $\alpha_G = 1$.
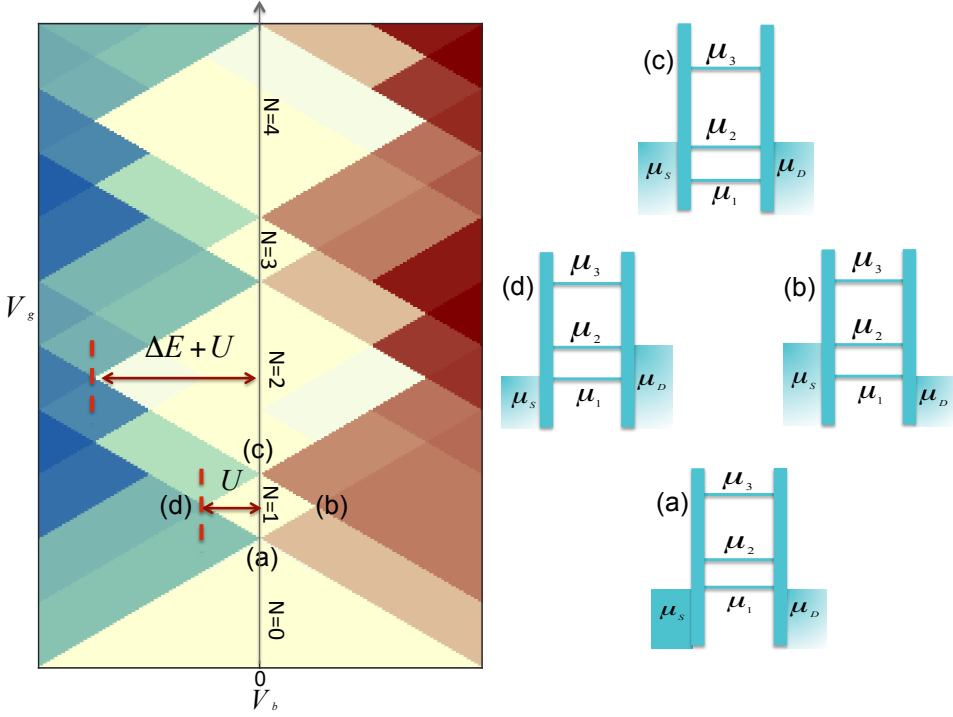
**Figure 2.3:** Schematic model for a charge stability diagram, spin-degenerate system, Where the current is shown as a function of the bias and gate voltages. Here the bias is changed symmetrically. Within the light yellow areas, Coulomb diamonds, the number of electrons $N$ in the quantum dot is fixed due to the Coulomb blockade. The gate shifts all levels equally, with the value $V_g$. Chemical potential diagrams at different points (a-d) in the stability diagram are shown on the right part of the figure, where $\mu_N$ is the $N$th chemical potential. The current is calculated by Pauli master equation method that is described in Chapter 4

Note that the diamonds corresponding to an odd number of electrons are smaller since the additional energy is only the Coulomb interaction and for larger diamonds, the additional energy is the Coulomb interaction plus the difference between the the energy of the two single-particle energy levels, since spin down and spin up have the same energy. By increasing the bias, more than one electrochemical potential level is accommodated in the bias window whereby, as it can be seen in Fig 2.3 the current increase (darker blue and darker red) for larger bias voltage.

## 2.3 Double quantum dot, stability diagram

As discussed above, single QDs are sometimes regarded as artificial atoms, due to the discrete energy level structure and sometimes pronounced shell structure [9] for the electrons filling up the dot. Along the same line of reasoning, two coupled QDs, a double quantum
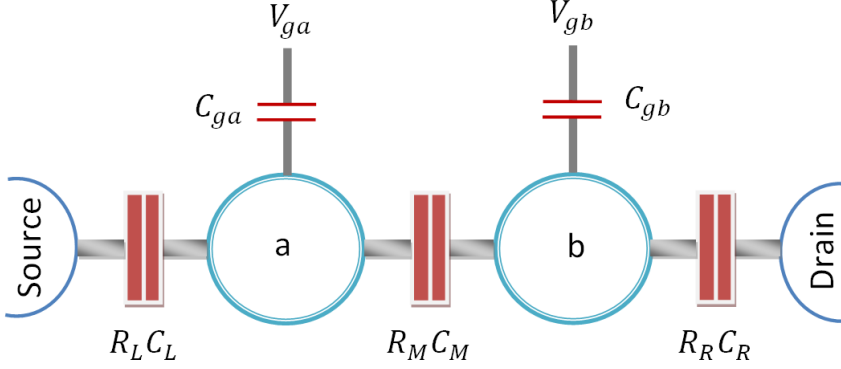
**Figure 2.4:** Schematic model for a double quantum dot system. This is a network of capacitors and resistors, indicating a double quantum dot system.

dots (DQDs), can be seen as artificial, di-atomic molecules. In contrast to real molecules, the properties of the artificial molecules can be modulated in a controlled way during an experiment. That is, both the level structure of each QD atom as well as the inter-dot coupling, the bonds between the atoms, can be tuned electrically.

In addition, when two (or more) QDs are coherently coupled, they give rise to a large number of intriguing physical phenomena due to the interplay of electron correlations, interference effects, etc. As a particularly prominent example, DQD system can constitute building blocks for quantum bits, qubits, based on both the charge and spin degrees of freedom [35, 38, 40–45]. Moreover, DQDs have been proposed as good candidates for the implementation of elements in other nano-devices both for optoelectronics and quantum technology applications as well as quantum systems in general [41, 42, 46].

For the purpose of this thesis, it is essential to understand electron-electron interactions in coupled quantum dots, especially when quantum circuit elements are going to be built [40]. We will, as a starting point, discuss the model in Ref. [35]. Figure 2.4 shows a schematic image of a DQD, where each dot is coupled to one lead and the other dot via a tunnel barrier described by a capacitor ($C_M$) and a (tunable) tunnel resistor ($R_M$). The two gate voltages $V_{ga}$ and $V_{gb}$ are coupled capacitively to dots $a$ and $b$ with capacitances $C_{ga}$ and $C_{gb}$, respectively. Thus, the interdot coupling and the potential on each dot can be controlled separately.

The number of electrons in dot $a$ and $b$ is denoted by $n_a$ and $n_b$, and the corresponding charge state in the DQD by $(n_a, n_b)$. In the same way as we discussed for single quantum dot, the DQD electrostatic energy is denoted by $E(n_a, n_b)$. The chemical potentials of the
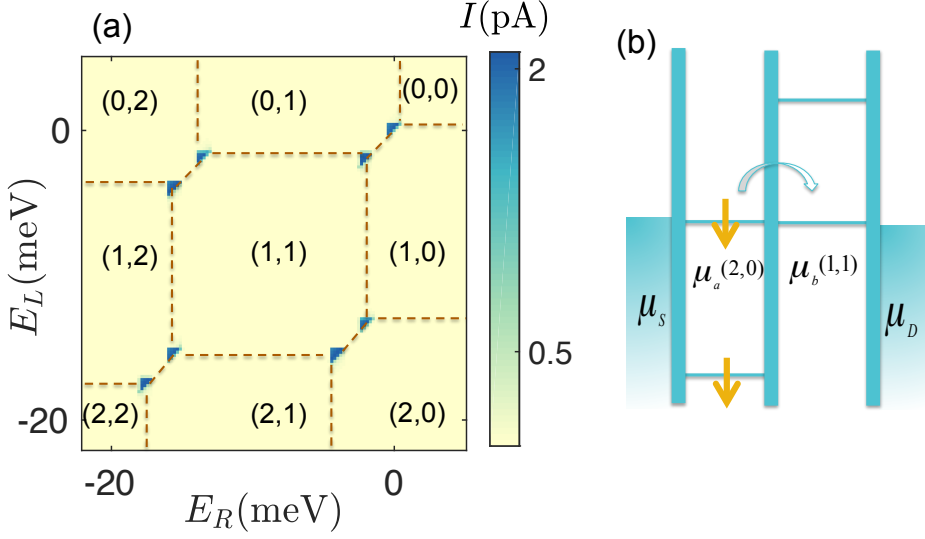
**Figure 2.5:** (a) Low bias stability diagram for a spin polarized double quantum dot system with the inter-dot tunnel coupling $\Omega$ = 0.02 meV, interdot interaction is $U$ = 10 meV and the bias is $V$ = 0.2 mV. The dashed lines, connecting triple points and separating charge stability regions, are a guide for the eye. (b) The schematic diagram for a specific transition from $(2,0)$ to $(1,1)$ is shown on the right side of the figure.

two quantum dots are defined by

$$\mu_a(n_a, n_b) = E(n_a, n_b) - E(n_a - 1, n_b)$$
$$\mu_b(n_a, n_b) = E(n_a, n_b) - E(n_a, n_b - 1). \tag{2.2}$$

In addition, dot a (b) is coupled to the source (drain) contact via another tunnel barrier, with a capacitance $C_L$ ($C_R$) and tunnel resistance $R_L$ ($R_R$). The applied source-drain bias $V_{SD} = V$.

Figure 2.5 schematically shows the low source-drain bias, linear response, conductance of a DQD as a function of gate voltages $V_{ga}$ or $V_{gb}$. It is assumed that each dot is coupled to its respective gate voltage $V_{ga}$ or $V_{gb}$, that controls the number of electrons. These kind of graphs are the *stability diagrams* for double quantum dot systems. This name comes from the fact that in the area where the transport of electrons is stopped, due to the Coulomb blockade, the double dot is in a stable charge state given by $(n_a, n_b)$. Electron transition through the DQDs can be understood as tunneling processes between many-body states in the dots. Based on this model, when the chemical potential in the right dot is aligned with the chemical potential in the left dot, both within the bias window, the states $(n_a, n_b)$, $(n_{a+1}, n_b)$, $(n_{a+1}, n_{b+1})$ are degenerate and sequential tunneling can take place. These regions of degenerate states are manifested as triple points, connections points between three lines in the stability diagrams.
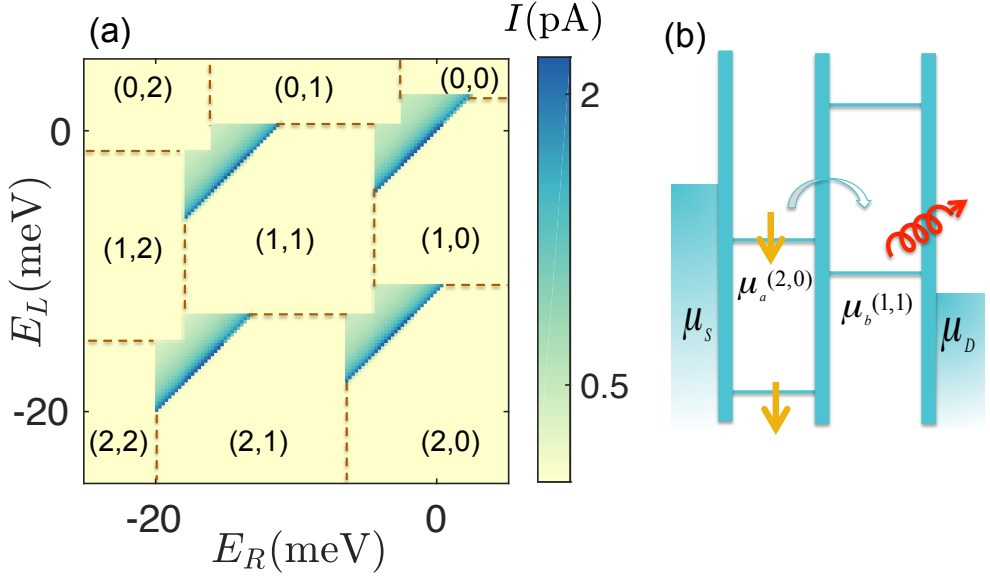
Figure 2.6: (a) Finite bias stability diagrams for a double quantum dot spin degenerate system, with the inter-dot tunnel coupling $\Omega = 0.02$ meV, intradot interaction is $U_n = 10$ meV, interdot interaction is $U_n = 3$ meV and the bias is $V = 5$ mV. Electron-phonon interaction is taken into account along the lines discussed in the transport part of the thesis. (b) The schematic diagram for a specific transition from $(2,0)$ to $(1,1)$ is shown on the right side of the figure. Though the energy level in the left dot is higher than the one in the right dot, electrons can transport through the right dot via emitting phonons. The phonon emission is illustrated by a curly red arrow.

## 2.4  Finite bias triangles and phonons

For finite source-drain voltage $V$, the triple points develop into bias triangles, the main topic of paper III. Inside the bias triangles, the Coulomb blockade is lifted and current can flow, As an illustrative example, the modification of the stability diagram in Fig. 2.5 due to finite $V$ is shown in Fig. 2.6. The reason for the current flow inside the bias triangle, is that electrons scatter inelastically when tunnelling between the dots. The origin of this inelastic tunnelling is typically phonons. As of now, we have neglected the coupling of the electrons in the QDs to vibrations of the atoms constituting the dots. In the quantum mechanical treatment employed here these lattice vibrations are described as phonons which couple to the motion of the electrons when tunneling between the dots. A microscopic description is given in the next chapter.

Some known physical effects, like nonlinearities in the current-voltage characteristic and conductance [4, 34, 47, 48], and some features in the DQD stability diagrams such as bias triangles [49–51], are caused by electron-phonon interactions. In general, electron-phonon interactions have strong effects on the electronics and optoelectronic properties

of the nanoscale structures, therefore, understanding the effects of these interactions is of fundamental importance.

The phonon modes are described by harmonic oscillators with energies $E = \hbar\omega(n + \frac{1}{2})$. In thermal equilibrium, the average number of phonons in a mode is given by the Bose-Einstein distribution

$$f_{\text{BE}} = \frac{1}{e^{\hbar\omega/k_B T} - 1},$$

(2.3)

where $k_B$ is the Boltzman constant and $T$ is the temperature. In this thesis, typically, the phonon temperature and hence the corresponding thermal energy is much lower than other relevant energy scales in the system. As a result, electron typically give away energy by creating phonons when tunneling. The opposite process, where tunneling electrons absorb energy from the phonons, is much less important. It is the inelastic tunneling events, when electrons tunnel under emission of phonons, that allow for current to flow in the entire bias triangle and not only under the condition of degenerate many-body states.

To illustrate this in more detail, we show in Fig. 2.6 the effect of electron-phonon interaction on the transport of electrons through a DQD system. The considered model is for a specific DQDs with arbitrary parameters sets given in the caption. A Pauli master equation approach is used to calculate the current, see chapter. 4 for a discussion of the transport models. Here we compare the stability diagrams for this double quantum dot system to the one in Fig. 2.5. For finite bias, the triple points in Fig. 2.5 grow out to finite size regions, bias triangles in Fig. 2.6, in which the current flows.

Importantly, in the absence of inelastic scattering, the tunneling only happens if the electronic levels in the two dots are aligned. However, as it is seen in Fig. 2.6(b), by emitting (absorbing) a phonon the electron can tunnel also off resonance [35]. The triangles of finite current appear due to the phonon emission process. When the energy level in the left dot is higher than the one in the right dot, electrons in the left dot are able to transport through the right dot by emitting phonons. This process can happen as long as the energy levels are in the bias window. Thus the size of the triangles depends on the bias magnitude. The absorption of phonons does not play any role since $k_B T \ll eV$. We observe a pair of overlapping full bias triangles, for each transition, due to the inter-dot Coulomb interactions.

The energy difference due to phonon emission is given by $\Delta E = \hbar\omega$ where, $\hbar$ is the reduced Planck's constant, and $\omega$ is the frequency of the phonon involved. This energy is given to the phonons. The size of the bias triangles are typically set by the applied voltage $V$, but as discussed below and also in e.g. paper III, there are several effects that can modify the properties of the triangles and also give rise to fine structures and regions of different currents inside the triangles.

## 2.5   Double quantum dots, Pauli spin blockade

In the description so far there has been no account for the spin properties of the electrons. However, in the DQD systems, electrons in the dots obey the spin selection rules which state that two electrons with the same spin cannot occupy the same orbital. Consequently, some specific configurations of electrons in DQDs will lead to a current blockade phenomenon, different from the Coulomb blockade. This phenomenon is known as *Pauli spin blockade*, since it comes from the Pauli exclusion principle [50, 52, 53]. The occupation of the double quantum dot is shown by $(m, n)$, where m and n are the numbers of electrons in the left and right dot respectively. Spin blockade can happen in the transition from $(1, 1)$ to $(0, 2)$.

When the quantum dots are coupled to each other, because of the tunnel coupling, the wave functions of electrons are no longer localized on one QD. Therefore, when there is one electron on each dot, depending on the spin of electrons, the system can be either in a singlet, $S(1, 1)$, or triplet, $T(1, 1)$, state. There is almost no difference between the energy of $S(1, 1)$ and $T(1, 1)$ states. However, there is a significant difference between the energy of $S(0, 2)$ and $T(0, 2)$. This energy difference comes from the fact that the electrons in the triplet state, $T(0, 2)$, have symmetric spin wave-function, and due to the Pauli exclusion principle, they can not occupy the same energy level; therefore, one of the electrons has to occupy an excited orbital. When there is one electron in the right dot and none in the left, the system is in the state $(0, 1)$. Because of an applied bias an electron can tunnel from the left lead to the left dot and set the system in a $(1, 1)$ state. Depending on the spin of the electrons, two possible configurations can ensue. The first case is when a spin singlet state $S(1, 1)$ is formed. In this case, the electron can tunnel through the right dot, since the singlet state $S(0, 2)$ is energetically accessible, and then through the right lead. The other possibility is that a spin triplet state $T(1, 1)$ is created. Since the electron spin is conserved during tunneling between the dots, the electron has to go from state $T(1, 1)$ to $T(0, 2)$. This transition is not possible since the triplet state in the right dot, $T(0, 2)$, has considerably higher energy, as, the energy difference between the ground and excited single-particle levels in the right dot is comparatively high. This process, the *Pauli spin blockade*, blocks the current and it is discussed in paper II and III in more detail.

## 2.6   Triple quantum dots

A triple quantum dot structure can, in analogy to the DQDs, be seen as more complicated, tri-atomic, molecules. In particular, triple quantum dots can have different kinds of geometries, such as a chain, a ring or a triangular shape. Various shapes have been extensively studied both theoretically and experimentally [54–63]. In paper I we focus on a linear,
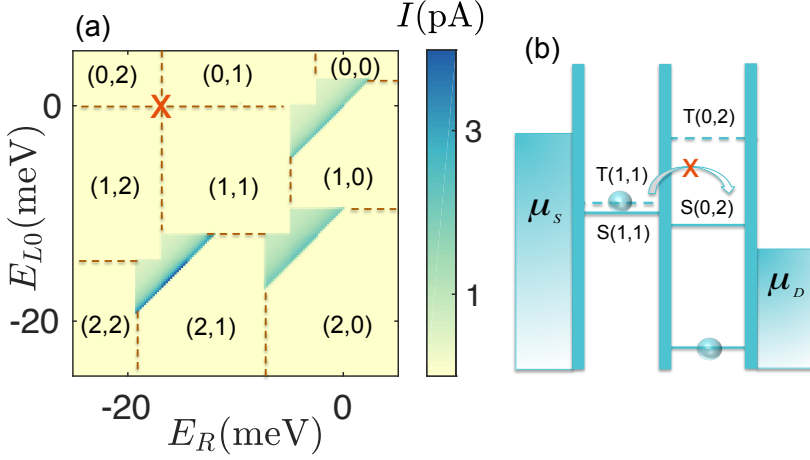
Figure 2.7: (a) Stability diagram for a spin degenerate double quantum dot system, with the inter-dot tunnel coupling $\Omega =$ 0.02 meV, intradot interaction is $U = 10$ meV, interdot interaction is $U_n = 3$ meV and the bias is $V = 5$ mV. The red cross denotes the region for the spin blockade. (b) Schematic diagram for a specific transition from $(1,1)$ to $(0,2)$ is shown on the right side of the figure. If the loaded state is parallel with the electron in the right dot, the tunneling is suppressed due to the $T(0,2)$ state being inaccessible in energy.

or chain geometry, with three QDs in series. Figure 2.8 shows such a triple QD system implemented in a nanowire [64] geometry and coupled to a source and a drain contact.

Experimentally a triple dot system can also be realized by a specific gate structure confining a two-dimensional electron gas [55, 65, 66] or a carbon nanotube [67]. It also serves as a model system for longer arrangements such as quantum dot superlattices [59] or possible dot-based quantum cascade lasers (QCLs) [68, 69]. The system that is shown in Fig. 2.8, was considered theoretically by B. Lassen and A. Wacker [54]. They analyzed the effect of Coulomb scattering on the transport of electrons through triple coupled dots. An important property is that the phase space restrictions in such low-dimensional structures reduce the scattering rates substantially, compared to bulk materials. This is one of the reasons for why triple dots have been suggested for a broad range of applications varying from quantum information processing [70] to quantum cascade lasers [68, 69]. Electron transport through these structures has also been widely used for level spectroscopy [35, 38, 71, 72] .

Generally, one assumes that the transport through quantum dot systems is governed by specific resonances. These happen due to the alignment of energy levels in different dots with those in neighboring dots, within the bias window of the system. This provides specific conditions for transport, which are resolved as current or conductance peaks for varying external parameters, such as the voltages at different gates. Such resonances may even refer to states with different energies due to the emission of phonons with a specified frequency [73, 74] or Auger processes [75]. However, even in this case, the existence of specific reson-
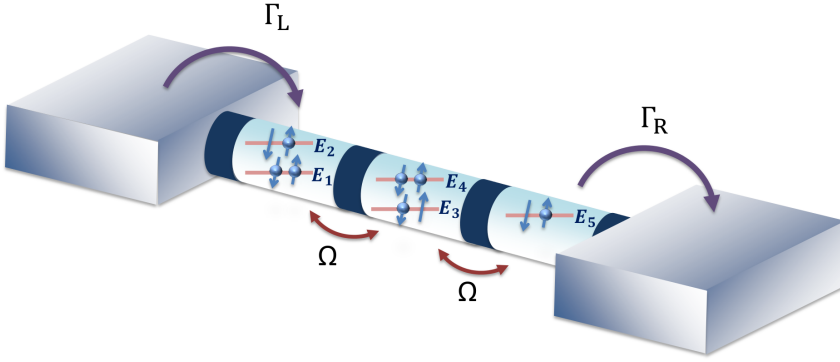
**Figure 2.8:** The triple quantum dot, implemented in a nanowire geometry, studied in paper I. The tunnel rates $\Gamma_L, \Gamma_R$ to the source and drain contacts and the interdot coupling strength $\Omega$ are shown.

ances is the guiding theme of studying multiple dot systems. However, with the increasing number of dots, the number of resonance conditions becomes large and difficult to satisfy simultaneously. Taking into account growth imperfections as well as undefined locations of impurities with fluctuating charges, a strong suppression of current is expected with an increasing number of dots [57, 58]. Electron-electron interaction is naturally occurring in all electronic devices and affects transport both by scattering (such as the Auger term) and level shifts.

In the first paper, we focus on charge transport through a serial arrangement of multiple quantum dots. The main interest of the work is to address the influence of different parts of the electron-electron (ee) interaction inside the triple-dot on the electrical current. We show that the Coulomb interaction between electrons opens up a large variety of different channels, which go far beyond the simple pictures of a few resonances, especially when the spin degeneracy of the levels is included.

# Chapter 3

# The nanostructure device model

The development, during the last decades, in design, fabrication and characterization of nanostructure devices have strengthened the need for studying the physics of open-quantum systems [76]. Simulating transport through such nanoscale systems is nontrivial, especially in the presence of strong electronic interactions that can lead to phenomena such as Coulomb blockade [37, 77] or the Kondo effect [78–80]. There are to date a large number of different theoretical methods to treat the transport, ranging from scattering approaches [81] via non-equilibrium Green's function techniques [82] to density matrix approaches [83–85].

To large extent is the approach taken depending on the properties of the nanostructure. For an open quantum system, with strong coupling between the nanostructure and the source-drain contacts and negligible electronic interactions, the modern theory of scattering, often referred to as Landauer-Büttiker theory [86, 87], is a commonly applied method due to its conceptual simplicity. Non-equilibrium Green's function techniques provides a framework to also account for interactions, such as electron-phonon or electron-electron ones. In this thesis we will focus on density matrix approaches, which are a natural choice for a nanosystem weakly coupled to source-drain contacts, where Coulomb blockade phenomena play an important role in the transport. A large variety of density matrix methods, including different types of master equations, have been developed [76, 83–85, 88–92].

The aim of this chapter is to discuss key aspects of the modelling of the serial QD systems, investigated by density matrix transport approaches used in all four papers I-IV. A general Hamiltonian for the QD-system will be introduced, where different parts of the many-body interaction are presented for this system. Moreover, rates for the coupling of the system to the source and drain contacts as well as to phonons will be derived and discussed. In this discussion concepts as many-particle states and the density operator will be introduced. In the next chapter we then discuss the density matrix approach to transport, based on the

results in the present chapter.

## 3.1 The Hamiltonian

The systems that are considered in this thesis consist of a number of serially coupled QDs that are connected to metallic leads. The following Hamiltonian can model such systems,

$$H = H_{\text{leads}} + H_{\text{dots}} + H_{\text{tunneling}}, \tag{3.1}$$

where, the first term describes the source and drain leads as reservoirs with a continuum of non-interacting electrons,

$$H_{\text{leads}} = \sum_{k\ell\sigma} E_{k\ell\sigma} c_{k\ell\sigma}^\dagger c_{k\ell\sigma}. \tag{3.2}$$

Here $c_{k\ell\sigma}^\dagger$ and $c_{k\ell\sigma}$ respectively create and annihilate an electron, with spin $\sigma = \uparrow, \downarrow$, in the lead $\ell$; $\ell = L, R$ stand for the left or right lead. Moreover, $k$ represents a continuous quantum number, which refers to the energy of the electrons $E_k$. This means that $k$-sums can be performed by introducing the density of states $\nu(E)$ as

$$\sum_k f_k \longrightarrow \int dE \nu(E) f(E). \tag{3.3}$$

where $f_k = f(E_k)$ is any given function. Also it is assumed that the energy of the lead states has a bandwidth $2D$, centered around the Fermi level. The particle energy $E_k \in [-D, D]$ and the density of states in this interval is a constant $\nu(E) \approx \nu(E_F) = \nu_F$. Then the $k$-sums are performed as $\sum_k f_k \longrightarrow \nu(F) \int_{-D}^{+D} dE\, f(E)$. Furthermore, $E_{k\ell} = E_k + \mu_\ell$ is the single-particle energy of the electron in state $k$. The dispersion $E_k$ in the lead is shifted by the chemical potential $\mu_\ell$ of the respective lead $\ell$. It is also assumed that the electrons in the leads are in thermal equilibrium with an electronic distribution characterized by a Fermi–Dirac function

$$f_\ell(E) = \frac{1}{1 + e^{(E-\mu_\ell)/k_B T_\ell}}, \tag{3.4}$$

with temperature $T_\ell$ and chemical potentials $\mu_\ell$.

The second term in Eq. (3.1), $H_{\text{dots}}$, is the many-body Hamiltonian that is used for the quantum dots,

$$H_{\text{dots}} = H_{\text{single}} + H_{\text{Coulomb}},. \tag{3.5}$$

Here first term, $H_{\text{single}}$, describes the single particle energies in each dot and the coupling between the states in the neighboring dots. This term is given by

$$H_{\text{single}} = \sum_{n\sigma} E_n d_{n\sigma}^\dagger d_{n\sigma} + \sum_{nm\sigma} \Omega_{nm} d_{n\sigma}^\dagger d_{m\sigma}, \tag{3.6}$$

where $d_{n\sigma}^{\dagger}$ ($d_{n\sigma}$) creates (annihilate) an electron with spin $\sigma$, in single-particle orbital $n$, and $\Omega_{nm}$ is the coupling between state $n$ in one dot and state $m$ in the neighboring dot, which are estimated by a standard tight-binding superlattice model [93]. The levels in one quantum dot only couple to the levels in the nearest-neighbor dots, and therefore the coupling matrix elements corresponding to the coupling between the levels in the next-nearest-neighbor dots are zero.

The second term in Eq. (3.5) is the $H_{\text{Coulomb}}$, which describes the electron-electron interactions and becomes relevant if more than one electron is confined in the system,

$$H_{\text{Coulomb}} = \frac{1}{2} \sum_{\substack{mnkl \\ \sigma\sigma'}} V_{mnkl} d_{m\sigma}^{\dagger} d_{n\sigma'}^{\dagger} d_{k\sigma'} d_{l\sigma}. \tag{3.7}$$

Here $V_{mnkl}$ are the Coulomb interaction matrix elements. The calculation of the Coulomb matrix elements for the systems that we have studied in this thesis will be described in more detail in section 3.2.

The last term in Eq. (3.1) is $H_{\text{tunneling}}$, related to the coupling between the dots and the leads,

$$H_{\text{tunneling}} = \sum_{n,k\ell\sigma} \left( t_{n,k\ell} d_{n\sigma}^{\dagger} c_{k\ell\sigma} + \text{h.c.} \right), \tag{3.8}$$

where $t_{n,k\ell}$ is the magnitude of the tunneling between the leads and the dots, and h.c. stands for the Hermitian conjugate. An important energy scale in the calculations is the tunneling rate between the dots and the source and drain contacts, defined as

$$\Gamma_{n,k\ell}(E) = 2\pi \sum_{n,k\ell} |t_{n,k\ell}|^2 \delta(E - \varepsilon_{k\ell}), \tag{3.9}$$

In our calculations the tunneling amplitude is assumed to be energy, or $k$, independent and therefore $t_{n,k\ell} = t_{n,\ell}$. In this case the tunneling rates become

$$\Gamma_{n\ell} = 2\pi \nu_F |t_{n\ell}|^2. \tag{3.10}$$

We note that in the case of single spinful orbital with on-site interaction $U$, the Hamiltonian Eq. (3.1) is referred to as an Anderson-type model [94–96]. This model has been intensively studied, for different kind of phenomena and in various parameter limits.

## 3.2   Matrix elements of the interactions

The Coulomb Hamiltonian operator, Eq. (3.7), describes the electron-electron interaction where $V_{mnkl}$ are the different matrix elements and in general reads

$$V_{mnkl} = \langle \chi_m | \chi_l \rangle \langle \chi_n | \chi_k \rangle \int d^3 r \int d^3 r' \varphi_m^*(\mathbf{r}) \varphi_n^*(\mathbf{r}') \frac{e^2}{4\pi \varepsilon_r \varepsilon_0 |\mathbf{r} - \mathbf{r}'|} \varphi_k(\mathbf{r}') \varphi_l(\mathbf{r}). \tag{3.11}$$

Here, $\varphi_m(\mathbf{r})$ and $|\chi_m\rangle$ are the spatial and the spin part of the single-particle state $m$, respectively. Also, $\varepsilon_r$ and $\varepsilon_0$ are the relative and vacuum permittivity, respectively. We neglect all terms, where either $m$ and $l$ or $k$ and $n$ belong to different quantum dots, as their overlap would be vanishingly small. Furthermore, terms connecting levels of next-nearest neighboring dots are small and neglected as well. The remaining terms can be categorized as *intradot* and *interdot* interactions depending on whether the two states are in the same dot or in two neighboring dots. These cases are separately treated below.

## 3.3    Intra-dot Coulomb matrix elements

For intradot interaction all the levels *mnkl* are considered to be in the same dot. By employing the normalization condition for the wave function, the direct elements can be estimated as

$$V_{mnnm} = \frac{e^2}{4\pi\varepsilon_r\varepsilon_0\sigma} = U, \qquad (3.12)$$

where $\sigma$ is the standard deviation for the spatial extension of the dot wave functions, $\sigma = \sqrt{\langle(\mathbf{r} - \langle\mathbf{r}\rangle)^2\rangle}$.

Another set of interaction matrix elements that have to be taken into account are $V_{mnmn}$ (for $n \neq m$), which act as exchange terms for equal spins and scattering terms for different spins. Trying different test wave functions (an example is discussed in 3.3.1) we observe

$$V_{mnmn} \approx U_{ex} = \frac{U}{5} \qquad (3.13)$$

This gives the correct order of magnitude of the exchange interaction $U_{ex}$ compared to the direct, on-site Coulomb interaction $U$, as is shown for example in paper III.

### 3.3.1    Matrix Elements for Harmonic Oscillator

As an illustrative example, we can evaluate the matrix elements by assuming Gaussian wave functions, eigenfunctions of the harmonic oscillator, as

$$\varphi_0(\mathbf{r}) = \frac{e^{-r^2/2a^2}}{(\pi a^2)^{3/4}}, \qquad \varphi_1(\mathbf{r}) = \frac{\sqrt{2}z}{a}\frac{e^{-r^2/2a^2}}{(\pi a^2)^{3/4}}, \qquad (3.14)$$

where $a = \sqrt{\hbar/m\omega}$ for a harmonic oscillator. Fourier transformation of Eq. (3.11) yields,

$$V_{mnkl} = \frac{e^2}{(2\pi)^3\varepsilon_r\varepsilon_0}\int d^3q \frac{A_{lm}^*(\mathbf{q})A_{nk}(\mathbf{q})}{q^2}$$

$$A_{nk}(\mathbf{q}) = \langle\chi_n|\chi_k\rangle\int d^3r\, e^{-i\mathbf{q}\cdot\mathbf{r}}\varphi_n^*(\mathbf{r})\varphi_k(\mathbf{r}). \qquad (3.15)$$

To find the relation between the magnitude of the direct term and exchange term, we calculate $V_{0110}$ and $V_{0101}$. From Eq. (3.14) and (3.15) we can find,

$$V_{0110} = \frac{e^2}{4\pi\varepsilon_r\varepsilon_0\sqrt{\pi/2a}}\frac{5}{6}, \qquad V_{0101} = \frac{e^2}{4\pi\varepsilon_r\varepsilon_0\sqrt{\pi/2a}}\frac{1}{6}. \tag{3.16}$$

Thus $V_{0101}$ is a factor 5 smaller compared to the direct term, which is just the result above in Eq. (3.13). This term acts as exchange interaction if electrons have the same spin and as a scattering term in case of two different spins.

## 3.4 Inter-dot Coulomb matrix elements

The direct interaction between two states in the neighboring dots can be evaluated in the same way as in Eq. (3.12), giving

$$V_{mnnm} = \frac{e^2}{4\pi\varepsilon_r\varepsilon_0 d} = U_n, \tag{3.17}$$

where d is the average distance between the two particles, which can be approximated by the distance between the centers of the dots. The terms with different combinations of indices are estimated by a Taylor expansion of $1/|\mathbf{r} - \mathbf{r}'|$ around the centers of the respective dots $\mathbf{R}_i$, $\mathbf{R}_j$, see ref. [97].

Defining $\mathbf{r}_1 = \mathbf{R}_i + \mathbf{s}$ and $\mathbf{r}_2 = \mathbf{R}_j + \mathbf{s}'$, where $\mathbf{s}$ and $\mathbf{s}'$ are the displacement of electron densities from the center of mass in dot $i$ and $j$, respectively. a Taylor expansion of the Coulomb interaction gives

$$\frac{1}{|\mathbf{R}_i + \mathbf{s} - \mathbf{R}_j - \mathbf{s}'|} = \frac{1}{|\mathbf{R}_i - \mathbf{R}_j|} - \frac{(\mathbf{R}_i - \mathbf{R}_j)\cdot(\mathbf{s} - \mathbf{s}')}{|\mathbf{R}_i - \mathbf{R}_j|^3} - \frac{(\mathbf{s} - \mathbf{s}')^2}{2|\mathbf{R}_i - \mathbf{R}_j|^3}$$
$$+ \frac{3(\mathbf{R}_i - \mathbf{R}_j)\cdot(\mathbf{s} - \mathbf{s}')(\mathbf{R}_i - \mathbf{R}_j)\cdot(\mathbf{s} - \mathbf{s}')}{2|\mathbf{R}_i - \mathbf{R}_j|^5}. \tag{3.18}$$

Using $|\mathbf{R}_i - \mathbf{R}_j| = d$ for neighboring dots, we find

$$V_{lnml} \approx \frac{e^2}{4\pi\varepsilon_r\varepsilon_0}\frac{\mathbf{s}_{nm}\cdot(\mathbf{R}_i - \mathbf{R}_j)}{d^3} = \pm U_{dc}, \tag{3.19}$$

The $U_{dc}$ term can be interpreted as a dipole-charge interaction that is the interaction between a superposition of two states in one dot and one specific state in the neighboring dot. In these matrix elements, the indices $n$ and $m$ represent the states in the same dot, whereas $l$ is the state in the next neighboring dot.
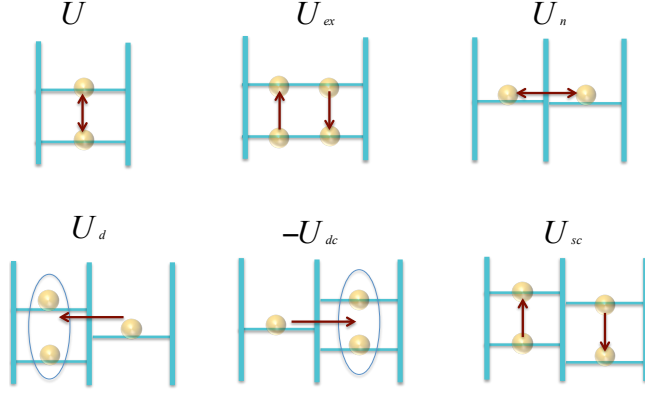
**Figure 3.1:** Schematic view of the Coulomb interactions, showing the six different terms discussed in the text.

We moreover have the element

$$V_{mnkl} \approx \frac{-e^2}{4\pi\varepsilon_r\varepsilon_0} \frac{2\mathbf{s}_{ml} \cdot \mathbf{s}_{nk}}{d^3} = U_{sc}, \qquad (3.20)$$

with the intradot dipole matrix element

$$\mathbf{s}_{nm} = \int d^3 r \varphi_n^*(\mathbf{r})\mathbf{r}\varphi_m(\mathbf{r}). \qquad (3.21)$$

The $U_{dc}$ and $U_{sc}$ terms can be interpreted as a dipole-charge interaction and dipole-dipole scattering terms, respectively. The $U_{sc}$ term is responsible for the Auger process and is crucial for the current flow in our system that we considered in the first paper. The sign of $U_{dc}$ in Eq. (3.19), depends on whether the charge is on the right or left side of the dipole. In Fig. 3.1 we provide an overview of all the six different Coulomb interaction terms discussed above.

## 3.5 Electron-phonon interaction

The phonons are modeled as non-interacting bosonic modes

$$H_{ph} = \sum_q \hbar\omega_q b_q^\dagger b_q, \qquad (3.22)$$

were $b_q^\dagger$ creates a phonon in a mode $q$. The electron-phonon interaction is given by

$$H_{e-ph} = \sum_{nm,q} g_{nm}^q d_n^\dagger d_m (b_{\bar{q}}^\dagger + b_q). \qquad (3.23)$$

with the matrix elements $g_{nm}^{q}$ and $\bar{q}$ indicating the complex conjugate state of $q$. The phonon coupling to the free electrons in the leads is very small compared to the electron-phonon coupling in the central region, see Ref. [98], therefore we only consider the electron phonon coupling in the dot.

We consider deformation potential coupling to the phonons, which is given by the divergence of the displacement following [99]. We can express the corresponding coupling matrix element for the first acoustic phonon mode coupled to the electrons via the deformation potential by

$$g_{nm}^{q1} = \int d^3r\, \Psi_n^*(\mathbf{r}) D\nabla \cdot \mathbf{u}_{q1}(\mathbf{r}) \Psi_m(\mathbf{r}). \tag{3.24}$$

Here $\mathbf{u}_{q1}(\mathbf{r})$ is the displacement and $D$ is the deformation potential coefficient. The elongation $\mathbf{u}_{q1}(\mathbf{r})$ is given by [99]

$$\mathbf{u}_{q1}(\mathbf{r}) \overset{q\to 0}{\sim} N_q[(1 - \nu\frac{q^2 r^2}{2})\,\mathbf{e}_z - i\nu q r\,\mathbf{e}_r + \mathcal{O}(q^3)]e^{iqz}, \tag{3.25}$$

where $\nu$ is the ratio between transverse contraction and longitudinal elongation in the stretching force direction, which is called the Poisson number. In the limit where $q \to 0$ one can get the linear dispersion relation $\omega_q = vq$ with $v = \sqrt{\frac{E}{\rho}}$, where $E$ is the Young's modulus and $\rho$ is the mass density.

Taking into account Eq. (3.24) and Eq. (3.25) we obtain

$$\begin{aligned} g_{nm}^{q1} &= \int d^3r\, \Psi_n^*(\mathbf{r}) D\Big((\frac{\partial}{\partial r} + \frac{1}{r})u_r + \frac{1}{r}\frac{\partial u_\theta}{\partial \theta} + \frac{\partial u_z}{\partial z}\Big)\Psi_m(\mathbf{r}) \\ &= \int d^3r\, \Psi_n^*(\mathbf{r}) D\Big(iqN_q(1-2\nu)e^{iqz}\Big)\Psi_m(\mathbf{r}) + \mathcal{O}(q^3). \end{aligned} \tag{3.26}$$

By using the normalization condition [100]

$$\frac{1}{V} = \int d^3r\, |\mathbf{U}_q(\mathbf{r})|^2 = \frac{\hbar}{2M\omega_q} \tag{3.27}$$

it can be found that

$$N_q = \sqrt{\frac{\hbar}{2LA\rho\omega_q}} = \sqrt{\frac{\hbar}{2LA\rho vq}}. \tag{3.28}$$

In the above expression, $A$ is the wire area and $L$ is the normalization length for the phonon modes. By inserting Eq. (3.28) into Eq. (3.26) we obtain

$$g_{nm}^{q1} = i\sqrt{\frac{\hbar q}{2LA\rho v}} D(1-2\nu) \int d^3r\, \Psi_n^*(\mathbf{r})\, e^{iqz}\, \Psi_m(\mathbf{r}). \tag{3.29}$$

We express the electron-phonon coupling matrix element, $g_{nm}^q = g(q)y_{nm}^q$, in terms of a state-independent overall strength $g(q)$ and a dimensionless coefficient $y_{nm}^q$, given by

$$g(q) = i\sqrt{\frac{\hbar q}{2LA\rho v}}D(1-2\nu)$$

$$y_{nm}^q = \int d^3r\,\Psi_n^*(\mathbf{r})e^{i\mathbf{q}\cdot\mathbf{z}}(\mathbf{r})\Psi_m(\mathbf{r}). \tag{3.30}$$

By assuming that $y_{nm}^q$ is $q$-independent (e.g. by choosing a characteristic value), we obtain

$$y_{nm}^q \approx y_{nm}, \quad y_{nm}^{\bar{q}} \approx \bar{y}_{nm} = y_{mn}^*. \tag{3.31}$$

We can quantify the coupling strength between the different phonon modes and the electronic states in the quantum dots by the phonon spectral density. We can thus collect all the energy dependence in the spectral density [74] as

$$J(E) = \sum_q |g(q)|^2 \delta(E - \hbar\omega_q). \tag{3.32}$$

# Chapter 4

# Density matrix transport model

Based on the Hamiltonian model of the nanostructure derived in the last chapter, we here describe the theoretical model for the transport used throughout the thesis, including in all papers I-IV. As was mentioned in the previous chapters, studying electronic transport in nanostructures (multiple quantum dot, molecules, etc.) in which quantum effects are relevant, is an important but also non-trivial task. To investigate transport properties, depending on the properties of the system many theoretical approaches have been used such as scattering theory [87], numerical-renormalization group [81], many-body methods [101], non-equilibrium Green's functions [82] and density matrix equation-based approaches, including master equations, [76, 83–85, 88–91]. In the papers of this thesis we apply one of the most common techniques, the generalized master equation-based approach.

In this chapter, we first describe the concept of a density matrix and it's use is motivated. Then, the two related transport approaches are described, the density matrix equation, or the generalized master equation, approach and the rate equation, or Pauli master equation approach. The latter is a limiting, simpler, case of the former, applicable when the coherence between states inside the nanostructure can be neglected. [76, 85, 102, 103]. In contrast to the density matrix equation, where the full quantum state of the system (the density matrix) is needed, in a rate equation only probabilities for state occupations are used.

## 4.1 The equation of motion

In order to derive the generalized master equation, we start to write the equation of motion of the system on density matrix form. A density matrix, or density operator, is one of the most important concepts in statistical quantum mechanics, introduced by J. von Neumann in 1927. The density matrix $\rho(t)$ describes a statistical mixture of pure quantum states and

can in general be written

$$\rho = \sum_j p_j |\psi_j\rangle\langle\psi_j| \tag{4.1}$$

where $p_j$ is a probability, with $\sum_j p_j = 1$ and $|\psi_j\rangle$ a quantum state of the system. Importantly, the set of states $\{|\psi_j\rangle\}$ does typically not constitute an orthonormal basis, it can be any number of non-orthogonal states. In particular, working in the energy eigenbasis of the system $\{|E\rangle\}$, one can in general write

$$\rho = \sum_{EE'} \rho_{EE'} |E\rangle\langle E'| \tag{4.2}$$

Thus, the density matrix is typically not diagonal, there are elements $\rho_{EE'}$. That is, it has non-zero elements which are npon-zero. These elements are referred to as *coherences*, and are of quantum mechanical origin, that is, they cannot be described in terms of probabilities to find the system in a given energy eigenstate. Sometimes it is convenient to work not in the energy eigenbasis but the eigenbasis of the density matrix itself. Since it is by definition a positive (semi) definite matrix it can be diagonalized as

$$\rho = \sum_i W_i |i\rangle\langle i|. \tag{4.3}$$

In this equation, $\{|i\rangle\}$ is the complete basis set of $\rho$ and $W_i$ is the probability to find the system in state $|i\rangle$.

Also accounting for the time dependence of $\rho(t)$, the von Neumann equation gives the dynamics of the density operator.

$$i\hbar\frac{d}{dt}\rho = -[\rho, H] \tag{4.4}$$

If a system can be separated into two uncoupled subsystems, for instance in our situation the leads and the dot, not connected via tunnel barriers, it is possible to factorize the density into a lead and a dot part, $\rho = \rho_{\text{leads}} \otimes \rho_{\text{dots}}$. When coupling the two subsystems via the tunneling Hamiltonian, $H_{\text{tunneling}}$ this is no longer possible, that is, the density matrix of the full system is no longer in a product state. However, one can obtain information about the dot properties only by tracing the total density matrix over the lead degrees of freedom, as

$$\rho_{\text{dots}}(t) = Tr_{\text{leads}}[\rho(t)], \tag{4.5}$$

where the the resulting density matrix of the dot, $\rho_{\text{dots}}$, is called a reduced density matrix. Importantly, if the total state of the system is a pure quantum state, the reduced density matrix typically describes a non-pure, or mixed, state. This illustrates one of the key properties and uses of density matrices.

In the thesis, we study tunneling through a small system such as multiple quantum dots, connected to leads. As it was discussed in Sec. 3.1 the Hamiltonian of such a system is defined by

$$H = H_{\text{leads}} + H_{\text{dots}} + H_{\text{tunneling}}. \tag{4.6}$$

We will take the approach to work in the many-body eigenbasis of the dot system. We thus diagonalize the Hamiltonian $H_{\text{dots}}$ and get the many-particle eigenstates $|a\rangle, |b\rangle, |c\rangle,...$ where we use the convention that a state $|a\rangle$ contains one particle less than the state $|b\rangle$, which in turn contains one less that $|b\rangle$, etc. We can then write the dot Hamiltonian as

$$H_{\text{dots}} = \sum_a E_a |a\rangle \langle a|. \tag{4.7}$$

In this many-particle basis, the Hamiltonian that describes the tunneling between the states in the leads and the dot, $H_{\text{tunneling}}$, can then be written

$$H_{\text{tunneling}} = \sum_{ab,kl\sigma} T_{ba}(kl\sigma)|b\rangle\langle a|c_{kl\sigma} + h.c.), \tag{4.8}$$

where $\sigma = \uparrow, \downarrow$ denotes the spin, $k$ labels the spatial wave functions of the contact states and $\ell$ denotes the lead ($\ell = L/R$ for the left and right lead, respectively). Also, $T_{ba}(kl\sigma)$ is the tunneling matrix element, which determines the transition rate between state $|a\rangle$ and $|b\rangle$ for transfering one electron in the state $kl\sigma$ of the leads to the dot. We note that the number of electrons in state $|b\rangle$, $N_b$, equals $N_a + 1$. The transition matrix element can be written

$$T_{ba}(kl\sigma) = \sum_n t_{nl}\langle b|d^\dagger_{n\sigma}|a\rangle, \tag{4.9}$$

where the index $n$ runs over the dots.

In terms of these quantities we can write the time-evolution of the density matrix elements using the von Neumann equation

$$i\hbar\frac{\partial}{\partial t}\rho^{[0]}_{ag,b'g} = \langle ag|H\rho - \rho H|bg'\rangle, \tag{4.10}$$

where $|bg\rangle = |b\rangle \otimes |g\rangle$ with $|b\rangle$ indicating the eigenstate of the dot Hamiltonian and $|g\rangle$ expressing the eigenstate of the lead Hamiltonian. Importantly, the superscript [0] indicates that it is the density matrix element to zeroth order in tunneling. In our equations we keep only the single-particle, sequential tunnelling events (first order in tunneling, denoted [1]) and neglect all higher order, co-tunneling, events. For instance, we have the density matrix elements

$$\begin{aligned}
\rho^{[0]}_{bg,b'g} &= \langle bg|\hat{\rho}|b'g\rangle \\
\rho^{[1]}_{bg-\kappa,ag} &= \langle bg-\kappa|\hat{\rho}|ag\rangle,
\end{aligned} \tag{4.11}$$

where, for shortness, $\kappa$ is a composite index

$$\kappa \equiv k, \ell, \sigma; \tag{4.12}$$

and we have

$$\begin{aligned}
|bg + \kappa\rangle &= |b\rangle \otimes c_\kappa^\dagger |g\rangle, \\
|bg - \kappa\rangle &= |b\rangle \otimes c_\kappa |g\rangle.
\end{aligned} \tag{4.13}$$

By solving the equation of motion, Eq. (4.4), we obtain the equations

$$\begin{aligned}
i\hbar \frac{\partial}{\partial t} \rho_{bg,b'g}^{[0]} &= (E_b - E_{b'})\rho_{bg,b'g}^{[0]} + T_{ba_1}(\kappa_1)\rho_{a_1 g,g+\kappa_1,b'g}^{[1]}(-1)^{N_{a_1}} \\
&+ T_{bc_1}(\kappa_1)\rho_{c_1 g,g-\kappa_1,b'g}^{[1]}(-1)^{N_b} - \rho_{bg,c_1 g-\kappa_1}^{[1]}(-1)^{N_{b'}} T_{c_1 b'}(\kappa_1) \\
&- \rho_{bg,a_1 g-\kappa_1}^{[1]}(-1)^{N_{a_1}} T_{a_1 b'}(\kappa_1),
\end{aligned} \tag{4.14}$$

and

$$\begin{aligned}
i\hbar \frac{\partial}{\partial t} \rho_{cg-\kappa,bg}^{[1]} &\approx (E_c - E_\kappa - E_b)\rho_{cg-\kappa,bg}^{[1]} \\
&+ T_{cb_1}(\kappa)\rho_{b_1 g,bg}^{[0]}(-1)^{N_{b_1}}\langle g|c_\kappa^\dagger c_\kappa|g\rangle \\
&- \rho_{cg-\kappa,c_1 g-\kappa}^{[0]}(-1)^{N_b} T_{c_1 b}(\kappa).
\end{aligned} \tag{4.15}$$

In order to have a particle current from the left lead into the dots, there should be an electron in the single-particle state corresponding to $\kappa$. The term $\langle g|c_\kappa^\dagger c_\kappa|g\rangle$ in Eq. (4.15) corresponds to this necessity. Moreover, a phase factor $(-1)^{N_b}$ is needed because of the order exchange of the lead with the dot operators, i.e., $c_\kappa(|b\rangle \otimes |g\rangle) = (-1)^{N_b}|b\rangle \otimes |g\rangle$.

Summing Eq. (4.14) and Eq. (4.15) over all the lead states $|g\rangle$ we get

$$\phi_{b,b'}^{[0]} = \sum_g \rho_{bg,b'g}^{[0]} \tag{4.16}$$

which are the elements of the reduced density matrix $\rho_{dot}$, and

$$\phi_{cb}^{[1]}(\kappa) = \sum_g \rho_{cg-\kappa,bg}^{[1]}(-1)^{N_b} \tag{4.17}$$

that explain the transformations of electrons from the leads to the quantum dot. Diagonal elements $\phi_{bb}$ present the probability that an electron occupies the state $|b\rangle$ in the dot, regardless of the state of the leads. The off-diagonal elements $\phi_{bb'}$ describe the quantum coherence resulting from the point that an electron can be in the two states $|b\rangle$ and $|b'\rangle$ at the same time. These elements lead to interference effects in electron transmission through two states in Quantum dots.

The equations of motion for [0] and [1] matrix elements read

$$i\hbar\frac{\partial}{\partial t}\phi_{b,b'}^{[0]} = (E_b - E_{b'})\phi_{b,b'}^{[0]}$$
$$+ T_{ba_1}(\kappa_1)\phi_{a_1 b'}^{[1]}(\kappa_1) + T_{bc_1}(\kappa_1)\phi_{c_1 b'}^{[1]}(\kappa_1) \qquad (4.18)$$
$$- \phi_{bc_1}^{[1]}(\kappa_1)T_{c_1 b'}(\kappa_1) - \phi_{ba_1}^{[1]}(\kappa_1)T_{a_1 b'}(\kappa_1),$$

and

$$i\hbar\frac{\partial}{\partial t}\phi_{cb}^{[1]}(\kappa) \approx (E_c - E_k - E_b)\phi_{cb}^{[1]}(\kappa)$$
$$+ T_{cb_1}(\kappa)\phi_{b_1 b}^{[0]}f_\kappa - \phi_{cc_1}^{[0]}T_{c_1 b}(\kappa)f_{-\kappa}, \qquad (4.19)$$

Here we also make an assumption that the level occupation in the leads are thermally distributed according to the Fermi-Dirac distribution and are unaffected by the coupling to the quantum dots. That gives rise to to the following approximation,

$$\sum_g \rho_{bg,b'g}^{[0]}\langle g|c_\kappa^\dagger c_\kappa|g\rangle \approx f_\kappa\,\phi_{bb'}^{[0]},$$
$$\sum_g \rho_{bg-\kappa,b'g-\kappa}^{[0]} \approx f_{-\kappa}\,\phi_{bb'}^{[0]}. \qquad (4.20)$$

which is used below.

## 4.2   First-order von Neumann approach

The conditions that are assumed for the stationary state, that is when the time evolution of the density matrix can be disregarded, is

$$i\hbar\frac{\partial}{\partial t}\phi_{bb'}^{[0]} = 0, \quad i\hbar\frac{\partial}{\partial t}\phi_{cb}^{[1]}(\kappa) = 0, \qquad (4.21)$$

and we can write $\phi^{[1]}$ in terms of $\phi^{[0]}$ as

$$\phi_{cb}^{[1]}(\kappa) = \frac{T_{cb_1}(\kappa)\phi_{b_1 b}^{[0]}f_\kappa - \phi_{cc_1}^{[0]}T_{c_1 b}(\kappa)f_{-\kappa}}{E_\kappa - E_c - E_b - i\eta}. \qquad (4.22)$$

Now the 1vN approach equations can be obtained for the steady state from Eqs. (4.19), (4.21), and (4.22) as

$$
\begin{aligned}
0 = {}& \phi_{b,b'}(E_b - E_{b'}) \\
&+ \sum_{b''\ell} \phi_{bb''}\left[\sum_a \Gamma^{\ell}_{b''a,ab'}I^{\ell-}_{ba} - \sum_c \Gamma^{\ell}_{b''c,cb'}I^{\ell+*}_{cb}\right] \\
&+ \sum_{b''\ell} \phi_{b''b}\left[\sum_c \Gamma^{\ell}_{bc,cb''}I^{\ell+}_{cb'} - \sum_a \Gamma^{\ell}_{ba,ab''}I^{\ell-*}_{b'a}\right] \\
&+ \sum_{aa'\ell}\phi_{aa'}\Gamma^{\ell}_{ba,a'b'}\left[I^{\ell+*}_{b'a} - I^{\ell+}_{ba'}\right] + \sum_{cc'\ell}\phi_{cc'}\Gamma^{\ell}_{bc,c'b'}\left[I^{\ell-*}_{c'b} - I^{\ell+}_{cb'}\right].
\end{aligned}
\tag{4.23}
$$

In addition , we use the normalization condition for density matrix,

$$
\sum_b \phi_{bb} = 1
\tag{4.24}
$$

In Eq (4.23) the tunneling rate $\Gamma$ is defined as

$$
\Gamma_{ba,a'b'} = 2\pi\nu_F\sum_{\sigma}T_{ba}(l\sigma)T_{a'b'}(l\sigma),
\tag{4.25}
$$

Here the following integral was used

$$
2\pi I^{l\pm}_{ba} = \mathscr{P}\int_{-D}^{D}\frac{dE\,f(\pm E)}{E - p^l_{ba}} - i\pi\,f(\pm p^l_{ab})\theta(D - |p^l_{ba}|),
\tag{4.26}
$$

where $\mathscr{P}$ denotes the principal part and where

$$
p^l_{ba} = E_b - E_a - \mu_l, \quad f(E) = (exp[E/k_BT]+1)^{-1}
\tag{4.27}
$$

which results from applying the approximation of a flat, wide density of states, i. e, $\int_k \to \nu_F\int_{-D}^{D}dE$, with $\nu_F$ indicating the density of states at the Fermi level and $2D$ expressing the bandwidth of the leads. Hence, it is assumed that the largest energy scale in our calculations is the bandwidth of the leads.

Lastly, we are interested in the particle current from lead $\ell$ into the structure, $I_\ell$, which equals the rate of change of the occupation in the lead:

$$
\begin{aligned}
I_\ell(t) &= e\sum_{k\sigma}\frac{\partial}{\partial t}\langle c^\dagger_{k\ell\sigma}c_{k\ell\sigma}\rangle = e\sum_{k\sigma}\frac{\partial}{\partial t}\rho^0_{bg,bgk} \\
&= \frac{2e}{\hbar}\sum_{k\sigma}Im\left[T_{bc}(\ell\sigma)\phi^{[1]}_{cb}(k\ell\sigma)\right].
\end{aligned}
\tag{4.28}
$$

Here the current is formulated in terms of the off-diagonal elements of the total density matrix that connect two different states of the dot, the difference in occupation number of these states is one.

The current in the steady-state is achieved in terms of $\phi_{b'b}^{[0]}$ as

$$I_\ell = \frac{2e}{\hbar} \sum_{cb} Im \left[ \sum_{b'} \Gamma_{bc,cb'}^{\ell} I_{cb}^{\ell+} \phi_{bb'}^{[0]} - \sum_{c'} \Gamma_{bc,c'b}^{\ell} I_{cb}^{\ell-} \phi_{cc'}^{[0]} \right], \qquad (4.29)$$

as discussed in the first paper I.

## 4.3 Pauli master equation

Now we can obtain a rate, or Pauli master equation from the 1vN approach by ignoring the coherences $\phi_{bb'}$, $b \neq b'$. Taking into account the fact that the populations $P_b = \phi_{bb}$ we can write the time evolution for the occupation probability of a state $|b\rangle$.

$$\frac{dP_b}{dt} = \sum_{a\ell} \left[ P_a \Gamma_{a \to b}^{\ell} f^\ell(E_b - E_a) - P_b \Gamma_{b \to a}^{\ell} [1 - f^\ell(E_b - E_a)] \right]$$
$$+ \sum_{c\ell} \left[ P_c \Gamma_{c \to b}^{\ell} [1 - f^\ell(E_b - E_a)] - P_b \Gamma_{b \to c}^{\ell} f^\ell(E_c - E_b) \right]. \qquad (4.30)$$

where we have denoted $\Gamma_{a \to b}^{\ell} = \Gamma_{ab,ba}^{\ell}$, $\Gamma_{b \to a}^{\ell} = \Gamma_{ba,ab}^{\ell}$. To get the steady state conditions we put $dP_a/dt = 0$. Here, $P_a$, $P_b$, and $P_c$ are the probabilities that state $|a\rangle$, $|b\rangle$, and $|c\rangle$ are occupied respectively.

The first line in the above equation yields the rate at which the system turns to the state $|b\rangle$ from states $|a\rangle$ and $|c\rangle$. The first term corresponds to that the dot is in a state $|a\rangle$, with the probability $P_a$. Tunneling onto the dot would, therefore, be possible, if occupied states of matching the energy, $E_b - E_a$, could be found in the lead $\ell$. Due to the tunneling process, the state of the dot change from $|a\rangle$ to $|b\rangle$. The factor $f^\ell(E_b - E_a)$, indicates the probability that states with energies $E_b - E_a$ are occupied in lead $\ell$. The state $|b\rangle$ of the dot can also be reached if the state $|c\rangle$ is occupied, and an electron is removed to lead $\ell$. Similarly, electrons which leave the dot need empty states in the lead. The second term of the first line describes this tunneling process. The second row in the above equation describes the rate at which the system returns to state $|a\rangle$ and $|c\rangle$ from state $|b\rangle$. Where the first term and the second term contains the processes in which an electron leaves and enter the dot respectively.

Now we can evaluate the current in the steady-state from lead $\ell$ into the dot as

$$I_\ell = \frac{2e}{\hbar} \sum_{ab} \{ P_a \Gamma_{a \to b}^{\ell} f^\ell(E_b - E_a) - P_b \Gamma_{b \to a}^{\ell} [1 - f^\ell(E_b - E_a)] \}. \qquad (4.31)$$

## 4.4  Comparison of first-order von Neumann and Pauli approaches

In the previous sections of this chapter the derivation of the first-order von Neumann equation and the Pauli master equation was presented. In this section, we discuss in more detail their properties and the role of coherences. As discussed above, the off-diagonal elements of the reduced density matrix in the many-body eigenbasis of $H_{\text{dots}}$ are known as coherences.

The Pauli master equation approach ignores all such coherences. In contrast, the first-order von Neumann accounts for the coherences of the system and consider the tunnel transitions to the leads in the lowest order. The coherences are known to be of relevance, if $\Delta E \lesssim \Gamma$, where $\Delta E$ is the splitting between the many-particle states with the same number of particles and $\Gamma$ is the transition rate to the leads in units of energy. Typical examples for this situation have been already discussed in refs [104, 105].

The 1vN approach is considered to give reliable results if the temperature $k_B T$ of the leads exceeds the transition rate $\Gamma$, as shown by comparison with higher-order approaches [75]. For lower temperatures, $k_B T \sim \Gamma$, many-particle tunneling becomes important and one needs to go to higher order in tunneling [85]. Also, if $\Delta E \lesssim \Gamma$, the coherences are known to be of significance.

The Pauli master equation approach gives accurate results when the temperature is much larger than the coupling strengths $k_B T \gg \Gamma$. Furthermore, the levels of the dot must be well separated so that the effects of quantum superpositions, i.e., coherence, can be neglected. It should be mentioned that The Pauli master equation and the first order von Neumann (1vN) approaches give identical results if the coupling to the leads $\Gamma$ becomes vanishingly small compared to the level splittings, and non-diagonal elements of the density matrix are not relevant. However, in the case where $\Omega$, the coupling between the dots is less than $\Gamma$, coherences become essential, and the Pauli master equation is not reliable.

To put it in a nutshell, it is clear that the Pauli master equation is a reliable option if no coherences between different states develop. However, if coherences are essential, it is reliable to use the 1vN. Besides, both of these approaches are well-founded if only sequential tunneling is of relevance.

# Chapter 5

# Overview of the papers

## 5.1　Paper I

In this paper, we investigate the influence of electron-electron interactions on transport in three serial quantum dots sandwiched between metallic contacts (schematically shown in Fig. 2.8). In this system, only the right/left dot energy levels are directly connected to the leads with a continuum of levels. We find that the presence of single-particle resonances within neighboring levels are not essential, since the many-particle states create channels for the current flow under a wide range of configurations of single-particle levels.

To calculate the current we use the first-order von Neumann (1vN) approach [75, 76], that takes into account all density matrix elements and a simpler Pauli master equation which neglects coherences [104–107]. We also check the validity of the Pauli master equation by comparing it with the first-order von Neumann approach. Moreover, we neglect phonon-scattering here. Since the phonon scattering rates, between the states of the quantum dot, are of the order of $1/ns$ or even smaller [108–110], and such a scattering process can give current of at most $\approx 0.1$nA, which is found to be negligible. We calculate the current as a function of dot level energies $E_3$ and $E_4$ (see Fig. 5.1), for two different cases: (*i*) The spin-polarized system and (*ii*) The spin-degenerate system.

### 5.1.1　Spin polarized case

Figures 5.1(a) and 5.1(b) show the current as a function of $E_3$ and $E_4$, when all the interaction matrix elements except the scattering elements, $U_{sc}$, are zero. To calculate current we used the Pauli master equation and the first von Neumann approach for Fig. 5.1(a) and 5.1(b) respectively.
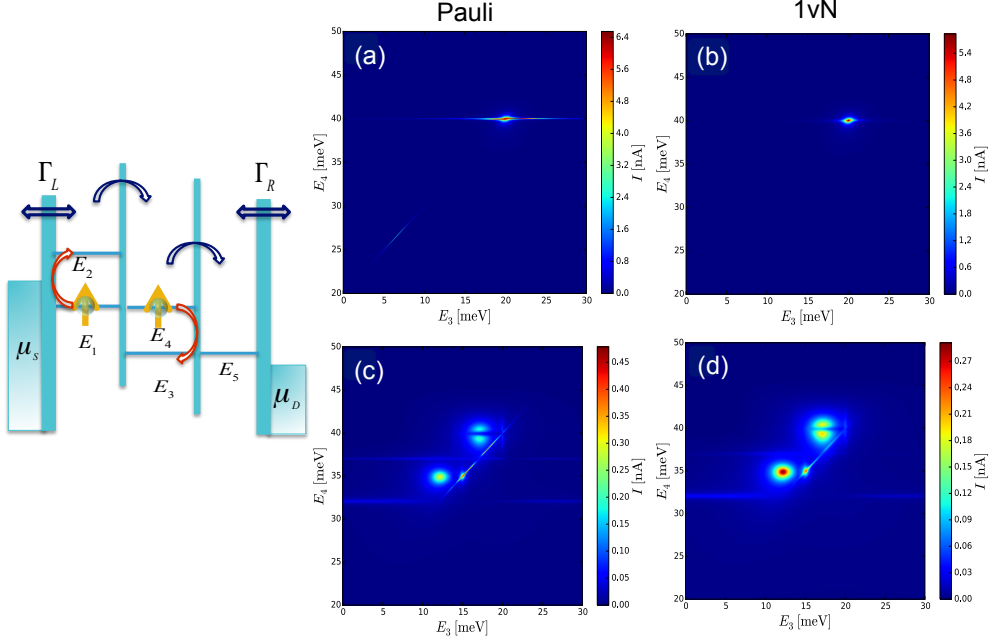
Figure 5.1: Spin-polarized system, (a),(b) with just scattering Usc included. (c),(d) All Coulomb matrix elements included. The two columns correspond to two different approaches. The diagram on the left shows schematically the energy levels

If the electrons occupy both levels 1 and 4, an energy-conserving scattering event creates the simultaneous transitions $1 \longrightarrow 2$ and $4 \longrightarrow 3$ (for $E_3 - E_4 = E_2 - E_1$ ), with subsequent tunneling to the right contact via the state 5. Therefore, the electrons are able to transfer through the system only if $E_3 = E_5 = 20\text{meV}$ and $E_4 = E_1 = 40\text{meV}$. Otherwise, the electron transport is blocked. On the other hand, by considering the full e-e interaction with all the interaction matrix elements, Fig. 5.1(c) and (d), the current flow is spread over a wide range of parameters, since a larger variety of excitation energies are relevant.

By comparing Fig. 5.1(c) and Fig. 5.1(d) we see that if all interactions are included the peak structure in the 1vN (Fig. 5.1(d))and Pauli (Fig. 5.1(c)) approaches is similar. However, the thin line of resonance for $E_4 \approx E_3 + 20$ is substantially reduced in the more advanced 1vN simulation. This reduction is the effect of the coherences developing between the many-body states which have energy differences smaller than the tunneling rate, $\Gamma$. Here, the relevant many-particle states are the 2-particle state occupying the levels 1 and 3, and the 2-particle state occupying levels 4 and 5, which are degenerate.

A similar pattern can be seen when just scattering $U_{sc}$ is included for spin-polarized levels Figs. 5.1(a) and (b), thin lines of resonances with high current appear at $E_4 \approx 40\text{meV}$ and $E_4 \approx E_3 + 20\text{meV}$ (faintly) for the Pauli master equation (Figs. 5.1(a)), however, for 1vN

approach the resonance is extending just along the $E_4 = 40\text{meV}$ line (Figs. 5.1(b)).

### 5.1.2    Spin-degenerate system

Figure 5.2 shows the result for the system with both spin species. Comparing Figs. 5.2(a) and (c) with Figs. 5.1(a) and (c) shows that the maximum of the current has increased by a factor of two. However, the behavior of the current in Fig. 5.2(a) that was calculated by the Pauli master equation is totally different compared to the 1vN approach Figs. 5.2(b). In Figs. 5.2(a) many resonances are noticeable, which totally reduced by the 1vN approach in Figs. 5.2(c). Furthermore, Fig. 5.2(b) shows that the resonance faintly extends along the intersection of $E_3 = 20\text{meV}$ and $E_4 = 40\text{meV}$. Though, in a spinless case, this resonance is just along the $E_4 = 40\text{meV}$ line.

In order to understand the reason for this difference, we look at the five one-particle eigenstates of the Hamiltonian responsible for transport. The plot on the right side of Fig. 5.2 shows a line for fixed $E_4 = 38\text{meV}$, and corresponding eigenstates are schematically shown in the squares. For specific parameters at the green (right) square, a significant current is observed for the spinful levels; however, the current is blocked for the spin-polarized levels. At the red (left) square, the current is blocked for both cases.

The superposition states $E_1$ and $E_4$ as well as $E_3$ and $E_5$ creates two new states with two new energies, which are referred to as $E_{1,4}$, $E_{4,1}$, $E_{3,5}$ and $E_{5,3}$. At the right (green) square ($E_2 - E_{1,4} \approx E_{1,4} - E_{3,5}$), therefore, the conservation of energy is satisfied, and the Coulomb scattering is possible. Only if the levels are spin degenerate, the Pauli principle can be fulfilled, and the electrons can transfer through the system. However, the current is blocked in a spin-polarized system. As it is illustrated on the right side of Fig. 5.2 if the coupling to the leads is enhanced, the current is decreased because of the to the coherences. Including all ee-interaction terms produces a broad variety of single-particle excitations. Therefore resonance conditions are easier to satisfy than Figures 5.2(c) and 5.2(d) show the evaluated current, and we observe a multitude of peaks as well as significant background current for a large number of energy level combinations.

Further, in this paper, we report that the principle part integrals in the 1vn approach, Eqs. (4.29), can give unphysical outcomes (current against the bias) which was the motivation for neglecting these terms in our calculations. See the supplementary information.

## 5.2    Papers II and IV

In the second paper, we report on the addition of phonon scattering to the QMEQ software [111], which is a package for numerical modeling of transport through quantum dot
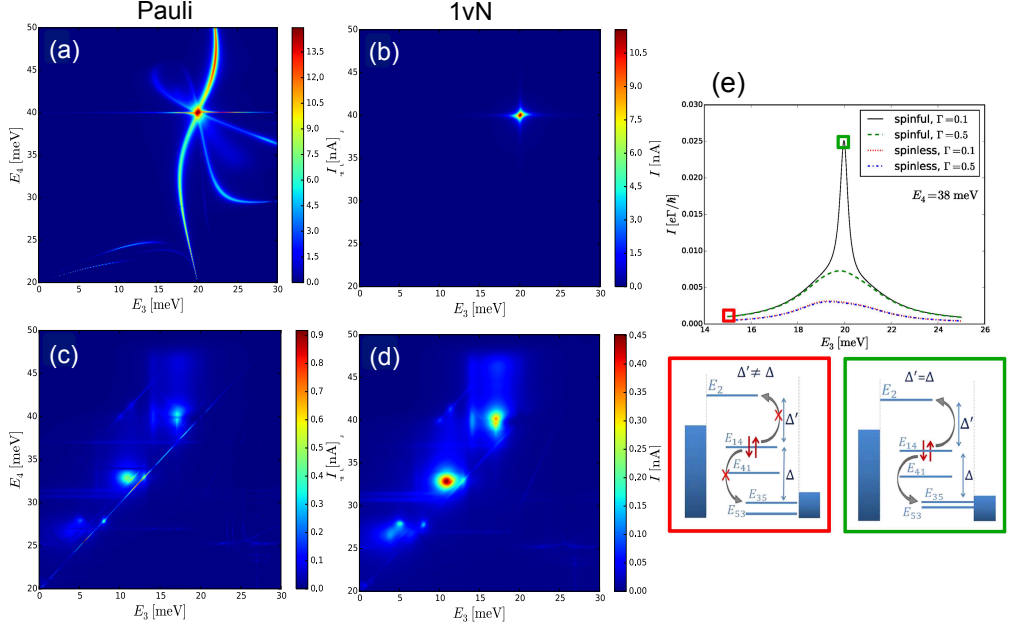
**Figure 5.2:** Two spin direction system, (a),(b) with just scattering $U_{sc}$ included. In (b),(d) all Coulomb matrix elements have been included. The two columns correspond to two different approaches. (e) Dashed (green) and dashed dotted (blue) gives current for larger coupling $\Gamma$ The left and right square panels show the one-particle eigenstates at two values of energy $E_3$.

systems based on density matrix equations. Here, we study a double-dot system with tunable energy levels, where energy relaxation is essential to match the energy levels difference, and compare our results to the experimental data in Ref. [74]. Furthermore, we show the particle current against the bias due to the non-equilibrium phonon distributions [112]. In order to calculate the electron-phonon interaction, I follow Sec. 3.5.

We used the Pauli master equation approach to calculate the current, In all the systems that we study here, $\Gamma$ is much smaller than the level splitting; therefore, the non-diagonal matrix elements of the density matrix do not play any role, and the first-order von Neumann approach gives the same result as the Pauli master equation[111, 113]. Fig. 5.3(a) and (c) show the current as a function of the left and the right dot energy levels ($E_L$ and $E_R$).

What can be seen is the rise of the current, close to the resonance line due to the phonon scattering. The bias triangles tell us that the current rises due to the phonon emission process. Since $k_B T \ll eV$, the phonon absorption does not play a role. On the left top of the Fig. 5.3(a) and (c), in the transition $(1,1) \longrightarrow (0,2)$, the current is suppressed due to Pauli spin blockade [50, 52]. Figure 5.3(b) shows schematically the configuration of the energy levels at this point. Figure 5.3(c) is different from Fig. 5.3(a) in the magnitude of
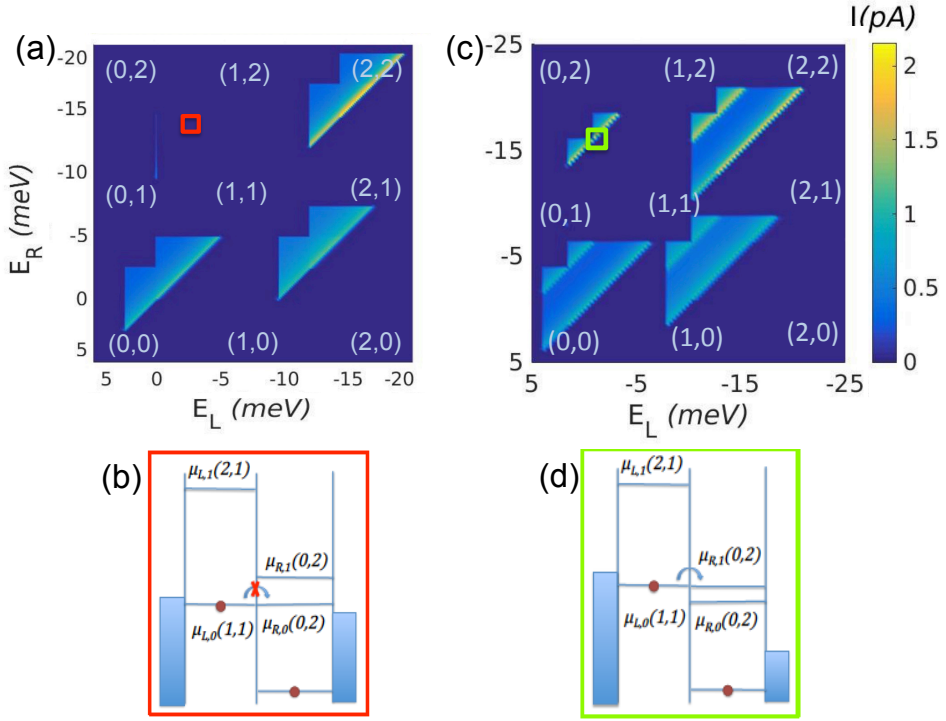
**Figure 5.3:** Stability diagrams of the double dot system. The bias is $V = 5$ mV. (b)The diagram shows schematically the removal energies $\mu_{i,n}(N_l, N_r)$ at the operation point denoted by red squares in (a). Due to Pauli spin blockade the current is suppressed at this point. [$\mu_{i,n}(N_l, N_r)$ is the energy of an electron removed from the level n (0 = ground, 1 = excited) of dot $i$ (left or right) where $N_{l/r}$ is the number of electrons in the left/right dot.] (c) Stability diagram with increased bias $V = 8$ mV, Here the combination of electron-phonon coupling and high bias lifts the Pauli spin blockade as sketched in panel (d)

bias. Since the bias in Fig. 5.3(c) is higher than in Fig. 5.3(a), both the ground and the excited states of the right dot can be in the bias window and the transition $(1,1) \longrightarrow (0,2)$ is possible via the excited state. Figure 5.3(d) shows the schematic diagram and depicts that energy level $\mu_{L,0}(1,1)$ can now be in resonance with $\mu_{R,1}(0,2)$, whereby the two-particle state $\mu_{R,0}(0,2)$ is emptied to the right lead.

In this paper, we also study the influence of a heated phonon distribution in the double dot system, which can operate as a heat engine [112, 114, 115]. The system that we have considered is a double dot system with one energy level in each dot. Figure 5.4(b) shows a schematic diagram of the system.

For this study, we fix the temperature of the electron leads to be $T_C = 60$ mK, but for the phonon distribution, we consider several different temperatures, $T_H$. The bias is zero, and the energy levels are tuned symmetrically. Figure 5.4(a) shows the current as a function of
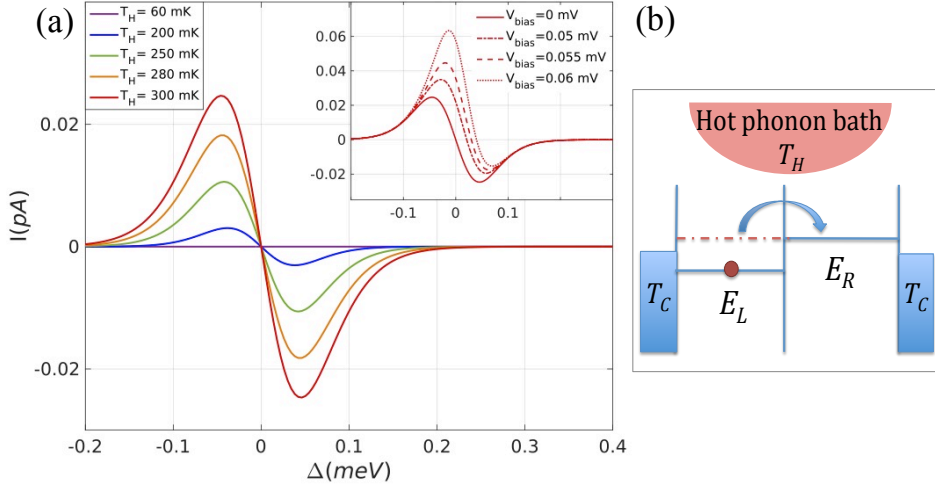
Figure 5.4: (a) Zero-bias current as a function of Δ, the difference between the energy levels of the dots, for different phonon temperatures. Inset: current as a function of Δ for different biases and $T_H = 300$ mK. Further parameter: $T_C = 60$ mK, $\Omega = 0.05$ meV, $\Gamma_L = \Gamma_R = 90$ neV. (b) A sketch of a double dot system coupled to non-equilibrium phonon bath.

Δ. Δ is the separation between the energy levels of the dots $\Delta = E_L - E_R$. It is apparent from this figure that the electrons can be transported through the system due to the asymmetry in the energy levels. An increase in the temperature $T_H$ will increase the current flow.

For the phonon bath with higher temperature, the phonon absorption dominates over phonon emission between the energy levels; therefore, electrons can transport through the system by acquiring heat from the phonons. The inset of Fig. 5.4(a) shows the current as a function of Δ for different values of the bias. As is illustrated the current can run against the bias, this process means that the system acts like a heat engine as it is discussed in Refs. [112, 114].

As we proposed in the second paper, there is a possibility of a phonon-assisted transport (PAT), through the DQD systems, even in the absence of the source-drain voltage. In this regard, the effect of a hot phonon bath on the transport through the DQD is investigated in paper IV, both experimentally and theoretically. The experimental setup contains InAs/InP nanowire DQDs with an external heat bath close to the DQD as a phonon bath and also two temperature sources for the left and right reservoirs, i.e., the source and the drain.

It is shown that the combination of the temperature gradient between the source and drain, and also the phonon bath, leads to a variety of the induced transport through the DQD system, which is characterized in this paper. Moreover, the spin relaxation in the PAT via excited states is also studied.
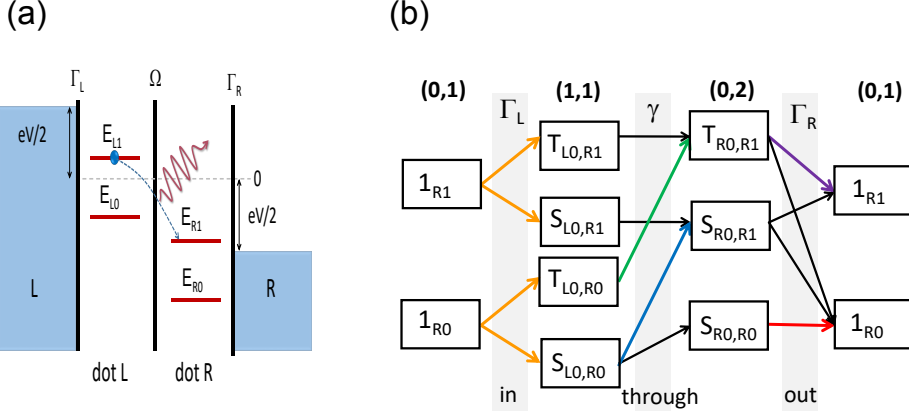
Figure 5.5: (a) Schematic of DQD-system, showing single particle energy levels $E_{L0}, E_{L1}, E_{R0}, E_{R1}$, tunneling rates $\Gamma_{L/R}$, inter-dot coupling $\Omega$ and the symmetric biasing, $\pm eV/2$, at each reservoir. An emission of a phonon in connection with an electron tunneling event (dashed line) is depicted with a wiggly, solid arrow. (b) available single and two-particle states (in black boxes) and transitions between them (solid, colored arrows), with corresponding rates

## 5.3 Paper III

In this work, we present a combined experimental and theoretical study of the nanowire DQD-device in Ref. [116]. We investigate the bias triangle features and identify features beyond the ones that are associated with excited dot states. By combining electrical current measurements, quantitative transport numerics, and a qualitative model, we predict and observe features, directly related to the inter-dot exchange energy, in triangles displaying Pauli spin blockade.

We used the Pauli master equation to calculate the current (Sec. 4.3), which is reliable since we only consider sequential tunneling and no coherences within various states develop. A schematic of the energy level structure of the nanowire DQD system is shown in Fig. 5.5(a). We consider two spin-degenerate single particle levels in each dot, denoted L0,L1 for the left (L) and R0,R1 for the right (R) dot, with corresponding energies $E_{\alpha n}$, $\alpha = $ L,R, $n = 0, 1$. The tunneling coupling between levels in different dots is $\Omega$. Moreover, the levels Ln (Rn) are tunnel coupled, with the same rate $\Gamma_L(\Gamma_R)$, to the left (right) electronic reservoir, respectively. The bias is applied symmetrically.

In this work we are only intested in the transition from $(1,1)$ to $(0,2)$ where the charge configurations $(1,1), (0,2)$ and $(0,1)$ are relevant. The states and transition chart corresponds to this charge configurations are shown in Fig. 5.5(b). Figure 5.6(a) shows the bias triangle as a function of energies $E_{L0}$ and $E_{R0}$. Also, a schematic bias triangle is shown in Fig. 5.6(c); each line in this figure corresponds to the same color arrow in Fig. 5.5(b). Since

the model is spin conserving, we focus on the bias triangle, where the Pauli spin blockade is lifted due to the applied bias. The Coulomb interaction between particles in different dots is large compared to the bias; therefore, we only analyze one triangle.

We are interested in the additional feature in the bias triangles, visible as a vertical dividing line between two regions of the different magnitude of the current. We show that the distance from this vertical line to the left border of the triangle is given by exactly $U_{\text{ex}}$. Since during the out-tunneling, $(0,2) \to (0,1)$, an electron tunnels out from an orbital $R0$ or $R1$ in dot R, to the right reservoir. There are four different out-tunneling processes, depicted with black, purple and red arrows in Fig. 5.5. The different processes occur with different energy constraints. Two processes are, however, crucial for the properties of the bias triangle. First, the transition $S_{\text{Ro,Ro}} \to R0$, denoted with a red arrow, is required for the transport cycle not to get blocked in the singlet state $S_{\text{Ro,Ro}}$. The corresponding energy constraint is

$$E_{\text{Ro}} > -eV/2 - U. \tag{5.1}$$

This gives rise to the vertical, red line $E_{\text{Ro}} = -eV/2 - U$ that can be seen in Fig. 5.6(c). Second the transition $T_{\text{Ro,R1}} \to R1$, denoted with a purple arrow Fig. 5.5(b), has an energy constraint
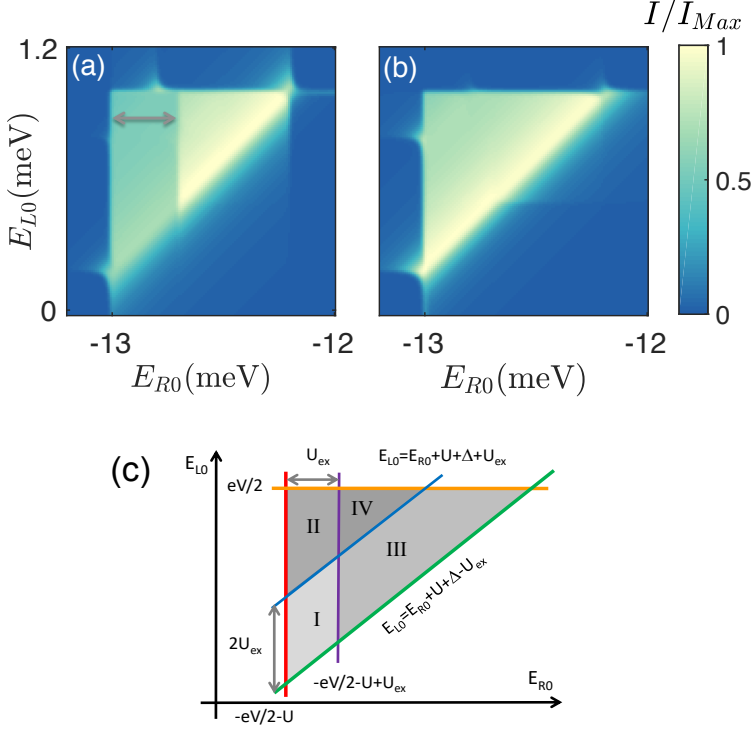
$$E_{\text{Ro}} > -eV/2 - U + U_{\text{ex}}, \tag{5.2}$$

giving rise to the purple line seen in the schematic bias triangle in Fig. 5.6(c), shifted $U_{\text{ex}}$ to the right with respect to the red line. We note that the intra-dot exchange leads to that spins singlets $S$ (triplets $T$), with one particle in R0 and one in R1, acquire an extra energy $+U_{\text{ex}} \, (-U_{\text{ex}})$.

We also find that there is another parameter that strongly affects the results, both qualitatively and quantitatively. That is the relation between the tunnel rates $\Gamma_{\text{L}}$ and $\Gamma_{\text{R}}$. Figure 5.6(b) illustrated the bias triangle for another set of $\Gamma_{\text{L}}/\Gamma_{\text{R}}$, for a constant product $\Gamma_L \Gamma_R$. The additional feature in the bias triangle is most present in the regime where $\Gamma_{\text{L}} \gg \Gamma_{\text{R}}$, and in the opposite regime, $\Gamma_{\text{L}} \ll \Gamma_{\text{R}}$, the corresponding bias triangle shows no additional features. The current flowing in the four different transport regimes, denoted with I-IV in Fig. 5.6(c), depends on the contributing tunneling processes.

To understand the currents in the different regimes and the corresponding bias triangle features, we analyze the different transport regimes in more detail by comparing the tunneling rates $\Gamma_{\text{L}}, \Gamma_{\text{R}}$, and $\gamma$ ($\gamma$ is the rate of the process where an electron tunnels and emits a phonon). We focus on the regime $\gamma \gg \Gamma_{\text{L}}, \Gamma_{\text{R}}$ corresponding to the experimental situation, the through-tunneling is much faster than the in and out-tunneling. As a consequence, the current in the different regimes can be written

$$I_{I/II} = 2e\frac{2\Gamma_{\text{L}}\Gamma_{\text{R}}}{(7/2)\Gamma_{\text{L}} + \Gamma_{\text{R}}}, \quad I_{III/IV} = 2e\frac{2\Gamma_{\text{L}}\Gamma_{\text{R}}}{2\Gamma_{\text{L}} + \Gamma_{\text{R}}}, \tag{5.3}$$

**Figure 5.6:** Electrical current as a function of energies $E_{L0}$ and $E_{R0}$, (a) Exchange energies $U_{ex} = 0.3$meV and $\Gamma_L/\Gamma_R = 0.1$ (b) Exchange energy is $U_{ex} = 0.3$meV and $\Gamma_L/\Gamma_R = 10$. (c) Bias triangle with limiting energy constraints shown with colored lines. Each line corresponds to one or more transfer processes, shown in the same color in Fig.5.5(a)

all independent of the rate $\gamma$, i.e. it is irrelevant for the current if the process $S_{L0,R0} \to S_{R0,R1}$, denoted by a blue arrow in Fig. 5.5, contributes to transport or not. This, in turn, gives that $I_I = I_{II}$ and $I_{III} = I_{IV}$ and that there is only one line in the bias triangle, a vertical separation between regions $I, II$ and $III, IV$.

Also, the result in Eq. (5.3) shows another interesting aspect. For an asymmetric coupling $\Gamma_L \gg \Gamma_R$, corresponding to the situation in the experiment, the currents in the two regimes become $I_{I/II} = e(8/7)\Gamma_R$ and $I_{III/IV} = e2\Gamma_R$, i.e. $I_{III/IV} = (7/4)I_{I/II}$. However, in the opposite regime, $\Gamma_R \gg \Gamma_L$, the two currents become the same, $I_{I/II} = I_{III/IV} = e4\Gamma_L$ and hence, the dividing line in the triangle disappears as can be seen in Fig. 5.6(b).

Our findings give a new way to determine the exchange interaction directly from the bias triangles. Moreover, we have shown that the existence of the features relies on strong electron-phonon interactions and asymmetry in the coupling strengths of the DQD to the left and right leads.

# Chapter 6

# Summary and outlook

In summary, in this thesis we have investigated various aspects of electronic transport in serially coupled quantum dots. This comprise electron-electron interaction induced transport channels in triple dot systems, the role of electron-phonon interactions and energy relaxation in double dots, novel bias triangle features in nanowire double dots and phonon and temperature induced heat and charge transport, also in nanowire double dots. In all of the works presented, paper I-IV, we have employed various density matrix methods to perform numerical calculations of the transport properties. Moreover, in paper II we presented a method development, by including electron-phonons interactions in an existing transport code. Two of the papers, III and IV, are in collaboration with experimental colleagues. In both papers III and IV we find a very good agreement between theoretical predictions and experimental results, suggesting that our numerical methods are well suited to describe transport in quantum dot nanostructures.

This observation, supporting the applicability of our density matrix approach to describe nanoscale electronic transport, also opens up a lot of possibilities for future research. To give a few interesting directions, the approach could be applied to a wide variety of energy and heat transport properties, of interest for nanoscale and quantum thermodynamics. These topics are presently attracting an increasing interest internationally and constitute an active area of experimental research in Lund. Moreover, by further developing the approach, one could include electron-photon interactions along the same line as electron-phonon interactions. This would open up for a broad spectrum of investigations of light-matter interactions, ranging from coherent coupling of coupling of tunneling electrons to microwave cavity photons to quantum dot based hot-electron solar cell devices. In addition, the available density matrix methods also allow for a theoretical investigations of time-dependent transport effects. Time dependent transport studies would provide interesting, novel results complementing the steady state properties at the focus of the present thesis.

# References

[1] A. I. Boukai, D. W. Tham, H. Liang, E. C. Hale, G. L. Kress, S. A. Steber, B. M. Wiles, and M. Chiasson, (2018).

[2] A. Wacker, Phys. Rev. B **66**, 085326 (2002).

[3] M. J. Biercuk, S. Garaj, N. Mason, J. M. Chow, and C. M. Marcus, Nano Lett. **5**, 1267 (2005).

[4] S. Sapmaz, C. Meyer, P. Beliczynski, P. Jarillo-Herrero, and L. P. Kouwenhoven, Nano Lett. **6**, 1350 (2006).

[5] M. T. Björk, B. J. Ohlsson, T. Sass, A. I. Persson, C. Thelander, M. H. Magnusson, K. Deppert, L. R. Wallenberg, and L. Samuelson, Appl. Phys. Lett. **80**, 1058.

[6] M. Björk, C. Thelander, A. Hansen, L. Jensen, M. Larsson, R. Wallenberg, and L. Samuelson, Nano Lett. **4**, 1621 (2004).

[7] M. A. Kastner, Rev. Mod. Phys. **64**, 849 (1992).

[8] L. P. Kouwenhoven, D. G. Austing, and S. Tarucha, Rep. Prog. Phys. **64**, 701 (2001).

[9] S. M. Reimann and M. Manninen, Rev. Mod. Phys. **74** (2002).

[10] B. J. Ohlsson, M. T. Björk, M. H. Magnusson, K. Deppert, L. Samuelson, and L. R. Wallenberg, Appl. Phys. Lett. **79**, 3335 (2001).

[11] D. G. Austing, S. Sasaki, S. Tarucha, S. M. Reimann, M. Koskinen, and M. Manninen, Phys. Rev. B **60**, 11514 (1999).

[12] S. Tarucha, D. G. Austing, T. Honda, R. J. van der Hage, and L. P. Kouwenhoven, Phys. Rev. Lett. **77**, 3613 (1996).

[13] M. A. Reed, R. T. Bate, K. Bradshaw, W. M. Duncan, W. R. Frensley, J. W. Lee, and H. D. Shih, J. Vac. Sci. Technol. **4**, 358 (1986).

[14] A. Ekimov, A. Efros, and A. Onushchenko, Solid State Commun. **56**, 921 (1985).

[15] J. M. Caruge, J. E. Halpert, V. Wood, V. Bulović, and M. G. Bawendi, Nat. Photonics **2**, 247 (2008).

[16] M. Grundmann and D. Bimberg, Jpn. J. Appl. Phys. **36**, 4181 (1997).

[17] C. Dang, J. Lee, C. Breen, J. S. Steckel, S. Coe-Sullivan, and A. Nurmikko, Nat. Nanotechnol. **7**, 335 (2012).

[18] M. H. Devoret, A. Wallraff, and J. M. Martinis, arXiv:cond-mat/0411174 (2004).

[19] J. M. Gambetta, J. M. Chow, and M. Steffen, npj Quantum Inf. **3**, 1 (2017).

[20] J. Claudon, J. Bleuse, N. S. Malik, M. Bazin, P. Jaffrennou, N. Gregersen, C. Sauvan, P. Lalanne, and J.-M. Gérard, Nat. Photonics **4**, 174 (2010).

[21] A. Kiraz, M. Atatüre, and A. Imamoğlu, Phys. Rev. A **69**, 032305 (2004).

[22] D. Tiarks, S. Baur, K. Schneider, S. Dürr, and G. Rempe, Phys. Rev. Lett. **113**, 053602 (2014).

[23] M. Ediger, G. Bester, A. Badolato, P. M. Petroff, K. Karrai, A. Zunger, and R. J. Warburton, Nat. Phys. **3**, 774 (2007).

[24] X. L. Liu, D. Hug, and L. M. K. Vandersypen, Nano Lett. **10**, 1623 (2010).

[25] M. Ciorga, A. S. Sachrajda, P. Hawrylak, C. Gould, P. Zawadzki, S. Jullian, Y. Feng, and Z. Wasilewski, Phys. Rev. B **61**, R16315 (2000).

[26] A. Zaslavsky, D. C. Tsui, M. Santos, and M. Shayegan, Appl. Phys. Lett. **58**, 1440 (1991).

[27] S. De Franceschi, J. A. van Dam, E. P. a. M. Bakkers, L. F. Feiner, L. Gurevich, and L. P. Kouwenhoven, Appl. Phys. Lett. **83**, 344 (2003).

[28] C. Fasth, A. Fuhrer, M. T. Björk, and L. Samuelson, Nano Lett. **5**, 1487 (2005).

[29] N. Mason, M. J. Biercuk, and C. M. Marcus, Science **303**, 655 (2004).

[30] H. J. Krenner, M. Sabathil, E. C. Clark, A. Kress, D. Schuh, M. Bichler, G. Abstreiter, and J. J. Finley, Phys. Rev. Lett. **94**, 057402 (2005).

[31] E. A. Stinaff, M. Scheibner, A. S. Bracker, I. V. Ponomarev, V. L. Korenev, M. E. Ware, M. F. Doty, T. L. Reinecke, and D. Gammon, Science **311**, 636 (2006).

[32] Y. Chen, Y. Sun, J. Peng, W. Zhang, X. Su, K. Zheng, T. Pullerits, and Z. Liang, Adv. Energy Mater. **7**, 1700162 (2017).

[33] D. Jacobsson, F. Panciera, J. Tersoff, M. C. Reuter, S. Lehmann, S. Hofmann, K. A. Dick, and F. M. Ross, Nature **531**, 317 (2016).

[34] L. H. Yu, Z. K. Keane, J. W. Ciszek, L. Cheng, M. P. Stewart, J. M. Tour, and D. Natelson, Phys. Rev. Lett. **93**, 266802 (2004).

[35] W. G. van der Wiel, S. De Franceschi, J. M. Elzerman, T. Fujisawa, S. Tarucha, and L. P. Kouwenhoven, Rev. Mod. Phys. **75**, 1 (2003).

[36] D. V. Averin and K. K. Likharev, J. Low. Temp. Phys. **62**, 345 (1986).

[37] M. H. Devoret, D. Esteve, H. Grabert, G. L. Ingold, H. Pothier, and C. Urbina, Ultramicroscopy **42–44, Part 1**, 22 (1992).

[38] R. Hanson, L. P. Kouwenhoven, J. R. Petta, S. Tarucha, and L. M. K. Vandersypen, Rev. Mod. Phys. **79**, 1217 (2007).

[39] A. Svilans, A. M. Burke, S. F. Svensson, M. Leijnse, and H. Linke, Physica E **82**, 34 (2016).

[40] D. Loss and D. P. DiVincenzo, Phys. Rev. A **57**, 120 (1998).

[41] A. J. Landig, J. V. Koski, P. Scarlino, U. C. Mendes, A. Blais, C. Reichl, W. Wegscheider, A. Wallraff, K. Ensslin, and T. Ihn, Nature **560**, 179 (2018).

[42] F. A. Zwanenburg, A. S. Dzurak, A. Morello, M. Y. Simmons, L. C. L. Hollenberg, G. Klimeck, S. Rogge, S. N. Coppersmith, and M. A. Eriksson, Rev. Mod. Phys. **85**, 961 (2013).

[43] X. Mi, J. V. Cady, D. M. Zajac, P. W. Deelman, and J. R. Petta, Science **355**, 156 (2017).

[44] D. J. Mowbray and M. S. Skolnick, J. Phys. D: Appl. Phys. **38**, 2059 (2005).

[45] Y. Nakamura, Y. A. Pashkin, and J. S. Tsai, Nature **398**, 786 (1999).

[46] D. DiVincenzo and D. Loss, Superlattice. Microst. **23**, 419 (1998).

[47] N. B. Zhitenev, H. Meng, and Z. Bao, Phys. Rev. Lett. **88**, 226801 (2002).

[48] H. Park, J. Park, A. K. L. Lim, E. H. Anderson, A. P. Alivisatos, and P. L. McEuen, Nature **407**, 57 (2000).

[49] N. Shaji, C. B. Simmons, M. Thalakulam, L. J. Klein, H. Qin, H. Luo, D. E. Savage, M. G. Lagally, A. J. Rimberg, R. Joynt, M. Friesen, R. H. Blick, S. N. Coppersmith, and M. A. Eriksson, Nat. Phys. **4**, 540 (2008).

[50] A. C. Johnson, J. R. Petta, C. M. Marcus, M. P. Hanson, and A. C. Gossard, Phys. Rev. B **72**, 165308 (2005).

[51] M. Brauns, J. Ridderbos, A. Li, W. G. van der Wiel, E. P. A. M. Bakkers, and F. A. Zwanenburg, Appl. Phys. Lett. **109**, 143113 (2016).

[52] K. Ono, D. G. Austing, Y. Tokura, and S. Tarucha, Science **297**, 1313 (2002).

[53] J. Fransson and M. Råsander, Phys. Rev. B **73**, 205333 (2006).

[54] B. Lassen and A. Wacker, Phys. Rev. B **76**, 075316 (2007).

[55] L. Gaudreau, S. A. Studenikin, A. S. Sachrajda, P. Zawadzki, A. Kam, J. Lapointe, M. Korkusinski, and P. Hawrylak, Phys. Rev. Lett. **97**, 036807 (2006).

[56] L. Gaudreau, A. S. Sachrajda, S. Studenikin, P. Zawadzki, A. Kam, and J. Lapointe, AIP Conf. Proc. **893**, 857 (2007).

[57] I. Weymann, B. R. Bułka, and J. Barnaś, Phys. Rev. B **83**, 195302 (2011).

[58] C. Emary, Phys. Rev. B **76**, 245319 (2007).

[59] D. Schröer, A. D. Greentree, L. Gaudreau, K. Eberl, L. C. L. Hollenberg, J. P. Kotthaus, and S. Ludwig, Phys. Rev. B **76**, 075306 (2007).

[60] K. Grove-Rasmussen, H. I. Jørgensen, T. Hayashi, P. E. Lindelof, and T. Fujisawa, Nano Lett. **8**, 1055 (2008).

[61] T. Kuzmenko, K. Kikoin, and Y. Avishai, Phys. Rev. Lett. **96**, 046601 (2006).

[62] P. Trocha and J. Barnaś, Phys. Rev. B **78**, 075424 (2008).

[63] M. C. Rogge and R. J. Haug, Phys. Rev. B **77**, 193306 (2008).

[64] A. Fuhrer, L. E. Fröberg, J. N. Pedersen, M. W. Larsson, A. Wacker, M.-E. Pistol, and L. Samuelson, Nano Lett. **7**, 243 (2007).

[65] T. F. Watson, B. Weber, J. A. Miwa, S. Mahapatra, R. M. P. Heijnen, and M. Y. Simmons, Nano Lett. **14**, 1830 (2014).

[66] S. Amaha, W. Izumida, T. Hatano, S. Teraoka, S. Tarucha, J. A. Gupta, and D. G. Austing, Phys. Rev. Lett. **110**, 016803 (2013).

[67] K. Grove-Rasmussen, H. I. Jørgensen, T. Hayashi, P. E. Lindelof, and T. Fujisawa, Nano Lett. **8**, 1055 (2008).

[68] B. A. Burnett and B. S. Williams, Phys. Rev. B **90**, 155309 (2014).

[69] T. Grange, Appl. Phys. Lett. **105**, 141105 (2014).

[70] E. A. Laird, J. M. Taylor, D. P. DiVincenzo, C. M. Marcus, M. P. Hanson, and A. C. Gossard, Phys. Rev. B **82**, 075403 (2010).

[71] T. S. Jespersen, K. Grove-Rasmussen, J. Paaske, K. Muraki, T. Fujisawa, J. Nygård, and K. Flensberg, Nat. Phys. **7**, 348 (2011).

[72] T. Hatano, Y. Tokura, S. Amaha, T. Kubo, S. Teraoka, and S. Tarucha, Phys. Rev. B **87**, 241414 (2013).

[73] T. Brandes and B. Kramer, Phys. Rev. Lett. **83**, 3021 (1999).

[74] C. Weber, A. Fuhrer, C. Fasth, G. Lindwall, L. Samuelson, and A. Wacker, Phys. Rev. Lett. **104**, 036801 (2010).

[75] J. N. Pedersen, B. Lassen, A. Wacker, and M. H. Hettler, Phys. Rev. B **75**, 235314 (2007).

[76] H.-P. Breuer and F. Petruccione, *The Theory of Open Quantum Systems* (Oxford University Press, Oxford, 2002).

[77] S. De Franceschi, S. Sasaki, J. M. Elzerman, W. G. van der Wiel, S. Tarucha, and L. P. Kouwenhoven, Phys. Rev. Lett. **86**, 878 (2001).

[78] D. Goldhaber-Gordon, H. Shtrikman, D. Mahalu, D. Abusch-Magder, U. Meirav, and M. A. Kastner, Nature **391**, 156 (1998).

[79] S. M. Cronenwett, T. H. Oosterkamp, and L. P. Kouwenhoven, Science **281**, 540 (1998).

[80] M. Pustilnik and L. Glazman, J. Phys. Condens. Matter **16**, R513 (2004).

[81] F. B. Anders, Phys. Rev. Lett. **101**, 066804 (2008).

[82] Y. Meir and N. Wingreen, Phys. Rev. Lett. **68**, 2512 (1992).

[83] S. A. Gurvitz and Y. S. Prager, Phys. Rev. B **53**, 15932 (1996).

[84] J. König, J. Schmid, H. Schoeller, and G. Schön, Phys. Rev. B **54**, 16820 (1996).

[85] J. N. Pedersen and A. Wacker, Phys. Rev. B **72**, 195330 (2005).

[86] M. Büttiker, Phys. Rev. Lett. **57**, 1761 (1986).

[87] Y. Blanter and M. Büttiker, Phys. Rep. **336**, 1 (2000).

[88] Y. V. Nazarov, Physica B **189**, 57 (1993).

[89] S. Koller, M. Grifoni, M. Leijnse, and M. R. Wegewijs, Phys. Rev. B **82**, 235307 (2010).

[90] C. Timm, Phys. Rev. B **77**, 195416 (2008).

[91] J. Jin, X. Zheng, and Y. Yan, J. Chem. Phys. **128**, 234703 (2008).

[92] G. Schaller, *Open quantum systems far from equilibrium*, Vol. 881 (Springer, New York, 2014).

[93] A. Wacker, Phys. Rep. **357**, 1 (2002).

[94] Y. Meir, N. S. Wingreen, and P. A. Lee, Phys. Rev. Lett. **70**, 2601 (1993).

[95] P. W. Anderson, Phys. Rev. **124**, 41 (1961).

[96] H. Haug and A.-P. Jauho, *Quantum Kinetics in Transport and Optics of Semiconductors*, 2nd ed. (Springer, Berlin ; New York, 2007).

[97] W. W. Parson, *Modern Optical Spectroscopy* (Springer Berlin, 2007).

[98] N. S. Wingreen, K. W. Jacobsen, and J. W. Wilkins, Phys. Rev. B **40**, 11834 (1989).

[99] G. Lindwall, A. Wacker, C. Weber, and A. Knorr, Phys. Rev. Lett. **99**, 087401 (2007).

[100] M. A. Stroscio, K. W. Kim, S. Yu, and A. Ballato, J. Appl. Phys **76**, 4670 (1994).

[101] J. Fransson, O. Eriksson, and I. Sandalov, Phys. Rev. Lett. **88**, 226601 (2002).

[102] H. Bruus and K. Flensberg, *Many-Body Quantum Theory in Condensed Matter Physics* (Oxford University Press, Oxford, 2004).

[103] J. N. Pedersen and A. Wacker, Physica E **42**, 595 (2010).

[104] A. Wacker and A.-P. Jauho, Phys. Rev. Lett. **80**, 369 (1998).

[105] H. Callebaut and Q. Hu, J. Appl. Phys. **98**, 104505 (2005).

[106] J. M. Kinaret, Y. Meir, N. S. Wingreen, P. A. Lee, and X.-G. Wen, Phys. Rev. B **46**, 4681 (1992).

[107] D. Pfannkuche and S. E. Ulloa, Phys. Rev. Lett. **74**, 1194 (1995).

[108] U. Bockelmann and G. Bastard, Phys. Rev. B **42**, 8947 (1990).

[109] O. Agam, N. S. Wingreen, B. L. Altshuler, D. C. Ralph, and M. Tinkham, Phys. Rev. Lett. **78**, 1956 (1997).

[110] T. Nakaoka, E. C. Clark, H. J. Krenner, M. Sabathil, M. Bichler, Y. Arakawa, G. Abstreiter, and J. J. Finley, Phys. Rev. B **74**, 121305 (2006).

[111] G. Kiršanskas, J. N. Pedersen, O. Karlström, M. Leijnse, and A. Wacker, Comput. Phys. Commun. **221**, 317 (2017).

[112] B. Sothmann, R. Sánchez, A. N. Jordan, and M. Büttiker, New J. Phys. **15**, 095021 (2013).

[113] B. Goldozian, F. A. Damtie, G. Kiršanskas, and A. Wacker, Sci. Rep. **6**, 22761 (2016).

[114] J.-H. Jiang and Y. Imry, Phys. Rev. Appl. 7, 064001 (2017).

[115] O. Entin-Wohlman, D. Chowdhury, A. Aharony, and S. Dattagupta, Phys. Rev. B **96**, 195435 (2017).

[116] S. Dorsch, B. Dalelkhan, S. Fahlvik, and A. M. Burke, Nanotechnology **30**, 144002 (2019).